A thermodynamically consistent poro-visco-elastic model of the Extracellular Matrix.

Giulia Laura Celora[1]

Supervised by: Sarah Waters[1] and Sonia Antoranz Contera[2]

[1] Mathematical Institute, University of Oxford
[2] Clarendon Laboratory, Department of Physics, University of Oxford

Abstract. In tissues, cells are mainly surrounded by an extracellular matrix (ECM), a soft porous media mixed with interstitial fluid and made up of networks of polymer chains and charged protein. It is known that the physical and biochemical properties of the ECM play a role in determining cell behaviour. While many studies have focused on linking the elastic properties of the ECM, less effort has been put in understanding the effect of its viscous properties on cell response. In this work, a non-equilibrium thermodynamic theory is developed to describe the chemo-mechanical behaviour of the ECM, which is modelled as a poro-visco-elastic polyelectrolyte. By using classical non-equilibrium thermodynamics we derive a set of governing equations for the transport of interstitial fluid and the time-dependent deformation of the ECM. Two different constitutive models are proposed which differ in how elastic and viscous deformation are coupled. An experimental protocol is then proposed with the aim of validating and selecting the proper model for the ECM.

1 Introduction

In vitro studies have shown that ECM rigidity and shear stresses due to the flow of interstitial fluid can promote malignant phenotypes in a population of initially normal cells, impact on cell proliferation and differentiation [8]. Further experiments have shown that tumour development is often associated with a stiffening of the tissue compared to the surrounding healthy one [37]. This causes cells to be exposed to higher compressive stresses and the blood vessels to collapse, thus impeding the diffusion of substances in the extra-cellular environment. Hence, numerous therapies are less effective [42]. Based on such evidence, it is now widely accepted that, unlike originally thought, biological process are not simply regulated by biochemical signals but by the complex interplay of mechanical and chemical stimuli.

Given the different physical nature and scale of phenomena involved, coupling micro-environment and cell behaviours is a problem of high complexity.

This requires understanding processes occurring at different temporal and spatial scales and how they interplay to determine the macroscopic behaviour of a tissue, whether healthy or damaged. Despite experiments probing the micro-scale being possible [2,24], these are usually limited to controlled environments in contrast to *in vivo* conditions, where we can instead measure macroscopic properties of tissues. In order to extrapolate information on the environment that cells perceive from the data, we thus need quantitative models able to link the tissue and cellular scale. This requires the development of a theoretical framework able to capture both the biology and physics involved which must also be consistent with the known universal laws of nature [27]. Having such knowledge can lead to the development of novel therapies that target the cell micro-environment and thus change the current approach to drug design.

As discussed in Section 2, the ECM is a polyelectrolyte gel [41,42], i.e. an hydrogel with charged groups. Besides being largely present in the natural world, synthetic polyelectrolytes are currently employed for a wide range of applications, such as drug delivery, biomedical devices, scaffolds for tissue engineering and soft robotics [7,12,13,31]. Hence, there has been a growing interest in the soft matter community in understanding their behaviour and translating it into mathematical models. In particular, research has been focusing on the phenomena of swelling, i.e. large deformation due to absorption of water, and the diffusion, transport and release of a solution [15,16,23,43]. In these studies, polyelectrolytes are commonly modelled as poro-elastic material. However, with the development of new experimental techniques such as Atomic Force Microscopy (AFM), which test the local mechanical properties of a material, soft tissues and hydrogels have been found to be visco-elastic [30]. As their solid skeleton, i.e. polymer network, is deformed, this can change its conformation to a most entropically favourable one thus dissipating energy. Where purely elastic solids deform instantaneously, viscoelastic materials have time-dependent deformation due to the irreversible nature of the process.

Despite experimental evidence, theoretical studies on visco-elastic soft materials remain limited. Our work aims to develop a continuum mathematical model of the extracellular matrix which is consistent with the laws of thermodynamics and accounts for the poro-visco-elastic nature of ECM. Transport and electro-chemical phenomena due to the flow of interstitial fluid are also included and coupled to the time-dependent deformation of the ECM by the use of linear non-equilibrium thermodynamics. Despite the focus on soft tissues, our results can be more widely applied to the study of polyelectrolyte gels. At our present knowledge, there is no previous work in the literature capturing all these aspects in a non-equilibrium thermodynamics framework. In [41,42] Xue et al. develop a nonlinear poroelastic theory for ECM, which couples all three physical phenomena but does not include viscous dissipation. In [19], the authors couple mechano-electrophysiological effects including the viscous dissipation but neglect transport; Caccavo et al. [9] propose a poro-viscoelastic model for neutral hydrogel, thus excluding electrical effects.

As discussed in [24], there are spatial and time scales which allow us to study visco-elasticity and poro-elasticity independently. On one hand, nanoscale rheological testing with AFM give us information on the visco-elastic properties of the sample. In the case of tissues and hydrogels, the most common rheological model used to fit experimental measurement is the 1D *Standard Linear Solid* model[9,24], see Figure 1. The poro-elastic behaviour can instead be characterized by standard creep-relaxation test. In this case, Darcy's law is usually applied to estimate the hydraulic conductivity and thus characterise the transport of fluid in the material, which usually modelled as an hyper-elastic solid [24,34]. Even though we have a good understanding of the two phenomena independently, there has been little attention to investigating how the two couple.

Following a typical approach in the framework of large deformations, we will be using a multiplicative decomposition of the deformation gradient to account for the two phenomena simultaneously. Based on previous studies, we here propose two different decompositions. Instead of arbitrarily choosing one of the two, we here develop both approaches with the aim of identifying their differences and investigating how experimental tests can be used to select the most appropriate. At the best of our knowledge, this is the first time the two are systematically compared in the literature.

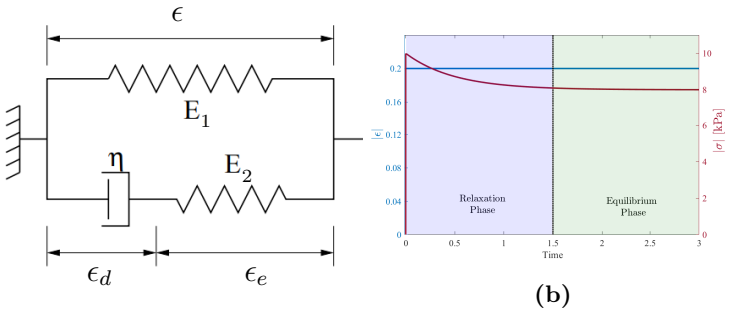

$$\begin{cases} \sigma = E_1\epsilon + E_2\epsilon_d \\ \dot{\epsilon}_e = \dot{\epsilon} - \frac{E_2}{\eta}\epsilon_e = \dot{\epsilon} - \frac{\epsilon_e}{\tau_R} \end{cases} \tag{1}$$

Fig. 1: 1D Standard Linear Solid. (a) Rheological Model; (b) Standard Response to a compression test. (1) Differential Equation for the Standard Linear Solid model in the 1D case.

Our work is organized as follows: in Section 2, we discuss more in details the composition of the ECM. We then present a brief overview of Classical Irreversible Thermodynamics, which focuses on the principles later used in Section 4 for the model derivation. Two different approaches to model the kinematics of the deformation are proposed and later compared in Section 6. As a result of our analysis, we suggest an experimental protocol which can allow us to validate and select the model that better represent the visco-elastic nature of the ECM.

2 Composition of Extracellular Matrix.

Despite the tissue-specific nature of extracellular matrix (ECM), this is usually composed of a network of collagen fibrils entangled with proteoglycans (PGAs) which are covalently bonded to charged chains of glycosaminoglycans (GAGs), see Figure 2a. While collagen is mainly responsible for the mechanical behaviour of the tissue, GAGs can imbibe water, giving the extracellular matrix the ability to swell while maintaining its structural integrity. As mentioned in the introduction, from this point of view, the ECM is a polyelectrolyte gel. As schematically illustrated in Figure 2(b), polyelectrolyte gels are 3D networks of cross-linked polymer chains that contain ionizable functional groups. When in solution the gel swells, while the functional groups dissociate into fixed charges and mobile ions in the solution. In particular, research has been focusing on the phenomena of swelling, i.e. large deformation due to the absorption of water, and the transport and release of a solution [15,16,23,43].

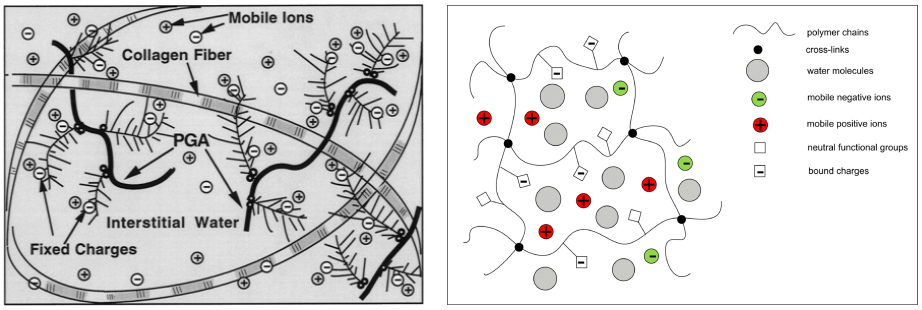

(a) **(b)**

Fig. 2: Analogy between ECM in soft tissue and polyelectrolytes hydrogels: (a) schematic diagram of the structure of the charged hydrated articular cartilage, reproduced from [39]; (b) an anionic polyelectrolyte gel modelled as a three-phase continuum, reproduced from [16].

For the purpose of this study, we will not explicitly distinguish between collagen, PGAs and GAGs. At the tissue level, this can be grouped into a single solid phase (the polymer network), whose mechanical properties are treated as the average over the different component contributions. The interstitial fluid is instead treated as a two-phase solution: the solvent (i.e. water) and the solutes (free ions). The transport of the solution also contributes to the dissipation of energy due to frictional forces generated by the relative motion of the different phases.

As is common in multiphase models of tissue, we will assume that the matrix is isotropic and GAGs are evenly distributed on the network. While this is not a good approximation for tissue like cartilage, which are highly anisotropic, it does apply to the extracellular matrix found in soft tissues such as liver, brain and tumours. It is also important to point out that the ECM has additional properties such as thermo-sensitivity and pH-sensitivity. However, both in living organisms and in experimental set-up temperature and pH are maintained fairly constant.

3 Non Equilibrium Thermodynamics.

As mentioned in the introduction, we are interested in studying the deformation of the ECM and the transport of solution in it. Since these are irreversible processes, they can not be described in the framework of equilibrium thermodynamics.

In the case of irreversible processes, the change in the entropy of a system $\mathrm{d}S$ results from both the reversible exchange of energy and matter with the external environment $\mathrm{d}_e S$ and the internal dissipation of energy during the process $\mathrm{d}_i S$ [27]:

$$\mathrm{d}S = \mathrm{d}_e S + \mathrm{d}_i S, \tag{2}$$

According to the second law of thermodynamics, which applies universally to any system or any of its sub-parts $\mathrm{d}_i S \geq 0$. It is important to notice that the second law allows transformations in which total change in entropy dS of the system is negative. This occurs whenever $\|\mathrm{d}_e S\| > \mathrm{d}_i S$, with $\mathrm{d}_e S < 0$, and it can lead to the spontaneous formation of complex and ordered structures such as living organisms. From this point of view, life emerges in physics as an efficient mechanism able to increase sufficiently the entropy of its environment [33].

In this study, we will focus on isothermal processes, i.e. $T = const$, as this well approximates physiological conditions well. Under this assumption, as derived by Gurtin in [21], the second law of thermodynamics is equivalent to the following *energy imbalance inequality*:

$$\frac{\mathrm{d}}{\mathrm{d}t}\left\{\int_R \psi\right\} \leq W(R) + M(R), \tag{3}$$

where R is an arbitrary control volume of the system, ψ is the Helmholtz free energy, $W(R)$ is the rate at which the environment does work on R and $M(R)$ is the inflow of mass due to transport. It is important to note that, as long as the quantities involved are well defined, the energy inequality (3) holds for any isothermal process independently of the specific physical system considered. This imposes a constraint on the form of the function ψ and its dependence on the other thermodynamic variables, such as temperature or pressure, which are used to describe the system.

Non-equilibrium thermodynamics mainly focuses on defining the form of $\mathrm{d}_i S$, which, unlike the reversible entropy production $\mathrm{d}_e S$, is not a state variable but depends on the specific transformation applied to the system. Different theories have been proposed, [27], each with its assumptions and specific domain of applicability. In our study we will focus on "Classical Irreversible Thermodynamics" (CIT) which was pioneered by Onsager [36] and Prigogine [38] in the first half of the 20th century. One the most important assumptions of this theory is the *Local Equilibrium Hypothesis*, which guarantees thermodynamic variables, including entropy, are locally well-defined, [27]. Consequently, we can introduce the entropy density $s = s(\mathbf{x}, t)$ such that:

$$S = \int_R s\,\mathrm{d}V, \qquad \mathrm{d}s = \mathrm{d}_e s + \mathrm{d}_i s, \qquad \mathrm{d}_i s > 0, \tag{4}$$

and the local entropy production:

$$\sigma \equiv \frac{\mathrm{d}_i s}{\mathrm{d}t} \geq 0. \tag{5}$$

Another central aspect of the theory is the introduction of *thermodynamic forces* [3] ζ_m (causes) and *thermodynamic fluxes* J_m (effects) to describe the time evolution of the system during an irreversible transformation. These are related to σ as follows:

$$\sigma = \sum_m \zeta_m J_m \geq 0. \tag{6}$$

While the local equilibrium hypothesis is at the basis of most theories of non-equilibrium thermodynamics, the following two hypotheses uniquely identify CIT:

1. *Linear Relation between forces ζ and fluxes J*:

$$J_m = \sum_k L_{mk}\zeta_k, \tag{7}$$

   where the constant L_{mk} are referred to as **phenomenological coefficients**;
2. *Microscopic Reversibility*: time reversibility of processes at the micro-scale.

Starting from these two principles, in his seminal paper [36] Onsager derives the well-known *Onsager Reciprocal Relation*:

$$L_{mk} = L_{km}. \tag{8}$$

If we now consider an isothermal transformation in the framework of CIT, alongside with the energy imbalance inequality, we have that the following must hold:

$$W(R) + M(R) - \frac{\mathrm{d}}{\mathrm{d}t}\left\{\int_R \psi\right\} = T\int_R \sigma \,\mathrm{d}V\,, \tag{9}$$

In the past few decades, CIT has been applied successfully to the modelling of several physical phenomena of interest for engineers, physicists and applied mathematicians. However, its validity is limited to phenomena near-equilibrium, for which a linear approximation of the flux-force relation holds. The growing interest in more complex far-from-equilibrium phenomena has pushed toward the development of a more general framework for the study of non-equilibrium phenomena. Since this goes beyond the purpose of our study, we will not discuss it further. We do, however, highlight the law of steepest entropy ascent, which, according to Beretta [4], seems to emerge as the fourth fundamental law of nature. In the linear regime, this principle can be used to prove Onsager's reciprocal relation [3], with no reference to the microscopic reversibility hypothesis, whose validity remains instead controversial [29].

[3] Not to be intended in the mechanical sense

4 Model Development

4.1 Conservation Law.

As mentioned in Section 2, we here consider the ECM as a three-phase medium composed of a solid polymer network with fixed charges, a solvent (i.e. water molecules, interstitial fluid) and solutes (freely moving charges).

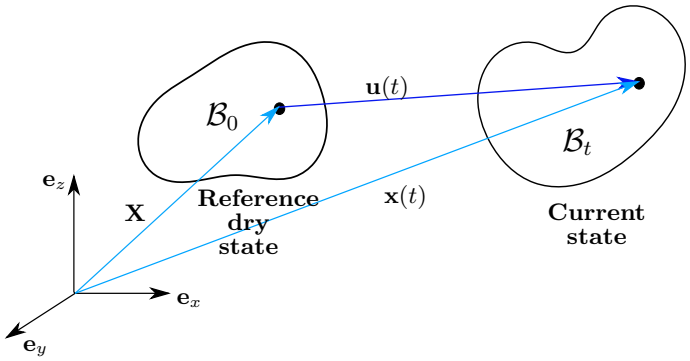

Fig. 3: Sketch of the dry and current state of the ECM network.

As the tissue deforms, the material element originally located at $\mathbf{X}$ in the initial configuration $\mathcal{B}_0$ is displaced to the point $\mathbf{x}$ in the current configuration $\mathcal{B}_t$, see Figure 3. Such a transformation is described by the deformation gradient tensor $\mathbb{F} = \partial\mathbf{x}/\partial\mathbf{X}$; the information about the change in ECM volume is encoded in $J = \det\mathbb{F}$, while $\mathbf{u} = \mathbf{x} - \mathbf{X}$ is the displacement vector. As in [22], we consider the reference, or initial, state $\mathcal{B}_0$, which is stress free, to be equivalent to the dry state of the ECM, i.e. only solid phase present. Since we assume the solid phase to be incompressible, any change in the volume can only be related to the migration of solvent and solute molecules, whose nominal [4] concentrations will be denoted by C_s and C_i respectively, $i = 1, \ldots, N$ with N being the number of free ion species. This lead to the molecular incompressibility condition:

$$J = 1 + v_s C_s + \sum_{i=1}^{N} v_i C_i, \tag{10}$$

where v_m are the characteristic molecular volume of each species in the solution. When considering the interstitial fluid, the contribution of ions to the volume can be neglected [41,42] so that Equation (10) reduces to:

$$J = 1 + v_s C_s. \tag{11}$$

Consequently, the volume fractions of fluid ϕ_f and solid ϕ_n phases in the swollen ECM are defined as:

$$\phi_f = \frac{v_s C_s}{1 + v_s C_s}, \qquad \phi_n = \frac{1}{1 + v_s C_s}. \tag{12}$$

[4] variable value in the reference configuration.

where again we are neglecting the contribution of ions to the total volume. While C_m denotes the number of each molecule per unit volume in the initial configuration for the m-th species in the solution, the actual concentration in the current state is denoted by $c_m = C_m/J$. Throughout the derivation of the model, we will be using the index $i = 1, \dots, N$ to denote the ionic species only, while $m \in \{s, 1, \dots, N\}$ refers to all mobile species, i.e. both the solvent and solutes.

Mass conservation must apply to all mobile species and in the initial configuration this reads:

$$\dot{C}_m + \nabla_0 \cdot \mathbf{J}_m = 0, \tag{13}$$

where $\mathbf{J}_m$ is the nominal flux per unit area in the dry state, $\dot{C}_m$ is the derivative of C_m with respect to time, i.e. $\dot{C}_m \equiv \partial_t C_m$ and ∇_0 denotes the gradient in the Lagrangian coordinates $\mathbf{X}$. Their counterparts in the actual configuration are denoted by $\mathbf{j}_m$ and ∇ and are defined according to the following rules:

$$\mathbf{J}_m = J\mathbb{F}^{-1}\mathbf{j}_m, \qquad \nabla_0(\cdot) = \mathbb{F}^T\nabla(\cdot). \tag{14}$$

When considering tissues or hydrogels, inertial and gravitational effects are commonly neglected, so that the conservation of momentum for the ECM reads:

$$\nabla_0 \cdot \mathbb{S} = 0, \tag{15}$$

where $\mathbb{S}$ is the first Piola-Kirchoff tensor, which represents the stress state of the ECM in the initial configuration. The counterpart in the current configuration is the Cauchy stress tensor $\mathbb{T}$, which is related to $\mathbb{S}$ as follows:

$$\mathbb{T} = J^{-1}\mathbb{S}\mathbb{F}^T. \tag{16}$$

The presence of free moving ions generates an electric field which is denoted by $\mathbf{E}$ and $\mathbf{e}$ in the initial and current configuration respectively. Introducing the electrostatic potential Φ, we have that:

$$\mathbf{E} = -\nabla_0 \Phi, \qquad \mathbf{e} = -\nabla \Phi. \tag{17}$$

As in [23], we consider the matrix to be a dielectric material[5]. Consequently, the presence of the electric field generates an electric displacement $\mathbf{H}$[6], which must obey Gauss law of electrostatics:

$$\nabla_0 \cdot \mathbf{H} = Q, \tag{18}$$

where Q is the local total charge, which accounts for both fixed and moving charges:

$$Q = e\left(\sum_i z_i C_i + z_f C_f\right), \tag{19}$$

[5] a material that does not conduct electricity but can be polarized in the presence of an electric field.

[6] the vector field that accounts for both the electric field and the polarization of the dielectric material.

where e is the elementary charge, C_f is the concentration of fix charges and z_m is the valence of the corresponding charged species. Note that C_f here corresponds to the concentration of GAGs, which is assumed to be a constant a fraction of C_s. As for above, we can move from nominal quantities to the corresponding value in the current configuration by applying the following rules:

$$\mathbf{H} = J\mathbf{h}\mathbb{F}^{-T}, \tag{20}$$

$$\mathbf{E} = \mathbb{F}^{T}\mathbf{e}, \tag{21}$$

where $\mathbf{h}$ is the electric displacement in the current configuration.

4.2 Kinematics.

As mentioned in the introduction, we model the ECM as a poro-visco-elastic material. As shown in Figure 4, there are two molecular processes that give rise to the macroscopic time-dependent response of the system:

1. the rearrangements of molecules at the micro-scale, which has entropic origin and results in a volume-preserving viscous deformation;
2. the long range transport of fluid that leads to swelling, i.e. changes in the ECM's size, and give rise to frictional forces between phases.

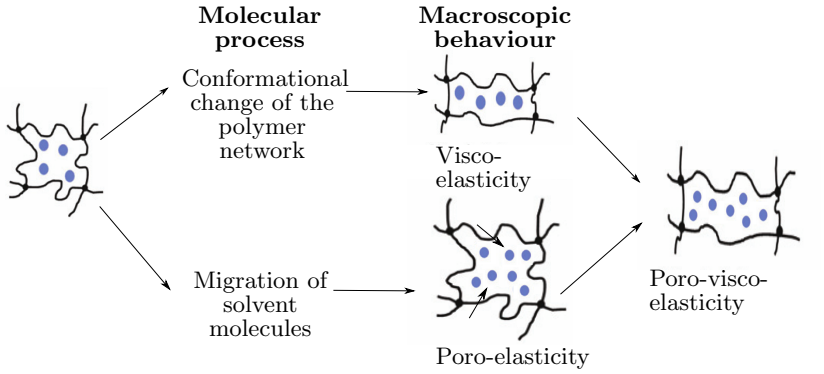

Fig. 4: Illustration of the molecular processes which account for the macroscopic deformation of ECM: viscosity is related to changes in the conformation of the network which preserve the volume of the network.

In order to capture both phenomena, as common in the large-deformation theory [1,9,10,20,35,40] and first proposed by Kröner in 1960 [28], we consider a multiplicative decomposition of the deformation tensor $\mathbb{F}$. As this can be chosen arbitrary, different decomposition have been proposed in the literature. These corresponds to different constitutive assumptions on the time-dependent

response of the material to deformation. For the purpose of this study, we consider the two most commonly used, which will be here denoted as model A [1,9,10] and model B [19,20,35]:

$$\text{MODEL A} \Rightarrow \begin{cases} \mathbb{F} = \mathbb{F}_e \mathbb{F}_v, \\ \det \mathbb{F}_v = 1, \quad \det \mathbb{F}_e = \det \mathbb{F}, \end{cases} \tag{A}$$

$$\text{MODEL B} \Rightarrow \begin{cases} \mathbb{F} = \bar{\mathbb{F}} \mathbb{F}_{vol} = \bar{\mathbb{F}}_e \bar{\mathbb{F}}_v \mathbb{F}_{vol}, \\ \det \mathbb{F} = \det \mathbb{F}_{vol}, \quad \det \bar{\mathbb{F}} = \det \bar{\mathbb{F}}_e = \det \bar{\mathbb{F}}_v = 1. \end{cases} \tag{B}$$

To the best of our knowledge, there is no previous systematic study in the literature that compares these two approaches. While the two model are identical in the case of iso-volumetric deformation, i.e. $\det \mathbb{F} = J = 1$, this is not always the case when a tissue swells, as it will be shown in Section (7.1).

For the purpose of the model derivation, we will derive in the main text only the governing equations for model A. The derivation of model B is analogous provided just minor changes, which are discussed in Appendix D.

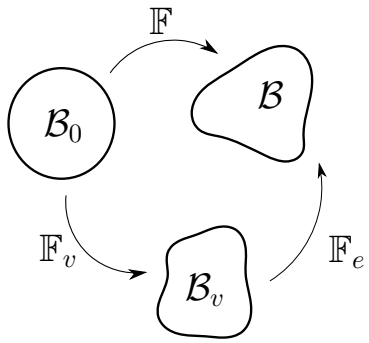

Fig. 5: multiplicative decomposition corresponding to model A, Equation (A).

Focusing on System (A), we identify $\mathbb{F}_e$ as the elastic contribution to the deformation while, the term $\mathbb{F}_v$ accounts for the viscous flow. As illustrated in Figure 5, the multiplicative decomposition is equivalent to introducing an intermediate configuration $\mathcal{B}_v$, called the natural or virtual configuration. The evolution of the natural configuration can be interpreted as an entropy producing, i.e. dissipative process. On the other hand, in the elastic deformation from the natural to the current configuration, all the energy is stored in the system.

Deriving Equation (A) with respect to time, we have that:

$$\dot{\mathbb{F}} = \dot{\mathbb{F}}_e \mathbb{F}_v + \mathbb{F}_e \dot{\mathbb{F}}_v \Longrightarrow \dot{\mathbb{F}}_e = \dot{\mathbb{F}} \mathbb{F}_v^{-1} - \mathbb{F}_e \mathbb{L}_v. \tag{22}$$

where $\mathbb{L}_v = \dot{\mathbb{F}}_v \mathbb{F}_v^{-1}$ is the viscous velocity gradient tensor. These can be decomposed into its symmetric $\mathbb{D}$ and skewed $\mathbb{W}$ part:

$$\mathbb{L}_v = \mathbb{D}_v + \mathbb{W}_v, \quad \mathbb{D}_v = \frac{\mathbb{L}_v + \mathbb{L}_v^T}{2}, \quad \mathbb{W}_v = \frac{\mathbb{L}_v - \mathbb{L}_v^T}{2}. \tag{23}$$

The decomposition (A) is not unique, as stress state in $\mathcal{B}_v$ would not change under any arbitrary rigid-body rotation [32]. As suggested by [1], in the case of an isotropic material, it is reasonable to assume the viscous flow to be irrotational, i.e. $\mathbb{W}_v = \mathbb{O}$, so that $\mathbb{L}_v \equiv \mathbb{D}_v$. As mentioned before, the physical nature of the viscous deformation is molecular rearrangement so that volume is preserved. This requires us to introduce the additional constraint:

$$J_v = \det \mathbb{F}_v = 1. \tag{24}$$

4.3 Energy Balance Inequality.

As mentioned in Section 3, in a thermodynamically consistent model, the free energy, ψ, can not be chosen arbitrarily but needs to satisfy the energy imbalance inequality, (3). In this section, we focus on the right-hand side of the inequality which specifies how the system exchanges energy and mass with the environment. Considering a control volume R in the reference configuration $\mathcal{B}_0$, the system exchanges mass due to the diffusion of each mobile species, so that $M(R)$ is given by:

$$M(R) = \sum_{m=s,1,\dots,N} - \int_{\partial R} \mu_m \, \mathbf{J}_m \cdot \mathbf{n}, \tag{25}$$

where $\mathbf{n}$ is the unit normal vector to the surface ∂R and μ_m is the chemical potential associated with each species. Widely used in the thermodynamics of mixtures, the chemical potential is a measure of the rate of change in free energy associated with adding one more molecule to a unit volume.

Following [16], the term $W(R)$, i.e. the rate of work done on the system, is decomposed into two contributions:

$$W(R) = - \int_{\partial R} \Phi \, \dot{\mathbf{H}} \cdot \mathbf{n} + \int_{\partial R} \mathbb{S}\mathbf{n} \cdot \dot{\mathbf{u}}, \tag{26}$$

which stands for the rate of electrical and mechanical work respectively. Substituting this result back into the formula (3) and applying the divergence theorem we obtain the following inequality:

$$\int_R \dot{\psi} - \mathbf{E} \cdot \dot{\mathbf{H}} + \sum_{i=1}^{N} \left[e\Phi z_i \dot{C}_i + \nabla_0 \left(\mu_i \mathbf{J}_i \right) \right] + \nabla_0 (\mu_s \mathbf{J}_s - \mathbb{S}^T \dot{\mathbf{u}}) \leq 0 \, . \tag{27}$$

Since the volume R can be chosen arbitrarily, the inequality must hold also locally:

$$\dot{\psi} - \mathbf{E} \cdot \dot{\mathbf{H}} + \sum_{i=1}^{N} \left[e\Phi z_i \dot{C}_i + \nabla_0 \left(\mu_i \mathbf{J}_i \right) \right] + \nabla_0 (\mu_s \mathbf{J}_s - \mathbb{S}^T \dot{\mathbf{u}}) \leq 0. \tag{28}$$

Further accounting for Equations (13)-(15), we obtain that:

$$\dot{\psi} - \mathbf{E} \cdot \dot{\mathbf{H}} + \sum_{i=1}^{N} \left[e\Phi z_i - \mu_i \right] \dot{C}_i - \mu_s \, \dot{C}_s - \mathbb{S} : \dot{\mathbb{F}} + \sum_m \nabla_0 \, \mu_m \cdot \mathbf{J}_m \leq 0. \tag{29}$$

As exhaustively discussed in previous studies [1,21], the energy inequality imposes restrictions on the constitutive equation of the free energy ψ. Adapting their results to our specific problem, we have that:

$$\psi = \psi(\mathbb{F}, \mathbb{F}_e, C_s, C_i, \mathbf{H}), \tag{30}$$

which precludes any explicit dependency of ψ on the chemical potentials μ_m or the viscous deformation gradient $\mathbb{F}_v$. By differentiating the incompressibility condition (11) and (24), we obtain:

$$v_s \dot{C}_s - J\mathbb{F}^{-T} : \dot{\mathbb{F}} = 0, \tag{31}$$

$$\mathbb{I} : \mathbb{L}_v = 0. \tag{32}$$

If we now substitute (30) and (22) into (29), and include the constraint (31)-(32) using as Lagrange multipliers p and p_v respectively, we are left with the augmented form of the energy imbalance inequality:

$$\begin{aligned} \left(\frac{\partial \psi}{\partial C_s} - \mu_s + p v_s\right)\dot{C}_s + \left(\frac{\partial \psi}{\partial \mathbf{H}} - \mathbf{E}\right)\cdot \dot{\mathbf{H}} + \sum_i \left(\frac{\partial \psi}{\partial C_i} + e\Phi z_i - \mu_i\right)\dot{C}_i \\ + \left(\frac{\partial \psi}{\partial \mathbb{F}} + \frac{\partial \psi}{\partial \mathbb{F}_e}\mathbb{F}_v^{-1} - \mathbb{S} - pJ\mathbb{F}^{-T}\right) : \dot{\mathbb{F}} + \sum_m \nabla_0 \mu_m \cdot \mathbf{J}_m \\ - \underbrace{\left(\mathbb{F}_e^T \frac{\partial \psi}{\partial \mathbb{F}_e} - p_v \mathbb{I}\right)}_{\mathrm{DEV}[\mathbb{M}_e]} : \mathbb{L}_v \leq 0, \end{aligned} \tag{33}$$

where $\mathbb{M}_e$ is the effective Mandel stress.

4.4 Construction of the Free Energy.

Having the general form of ψ, Equation (30), it remains to construct its precise form. Following a standard approach in ψ-depending modeling, we assume that the total free energy can be additively decomposed with each physical mechanism contributing independently. We here consider five distinct contributions:

- the energy of the electric field ψ_1;
- the energy of solvent and solutes' molecules not interacting with the solid phase ψ_2;
- the energy of mixing the solid phase with the solution, ψ_3;
- the energy of mixing the solvent with the solutes in solution, ψ_4;
- the energy of the solid phase not interacting with the solution, ψ_5.

Assuming the solid phase to be an ideal and linear dielectric material, with constant permittivity ϵ, the free energy of polarization reads [15,23]:

$$\psi_1 = \frac{1}{2\epsilon J}\mathbf{H}\mathbb{F}^T \cdot \mathbb{F}\mathbf{H}. \tag{34}$$

The specific energy density ψ_2 has the standard form:

$$\psi_2 = \sum_m \mu_m^0 C_m, \tag{35}$$

where μ_m^0 denotes the chemical potential of non interacting solvent and ions molecules. According to Flory-Huggins theory [17,25] of mixtures, the mixing energy is given by:

$$\psi_3 = \frac{k_B T J}{v_s} \left(\phi_f \ln \phi_f + \chi \phi_f \phi_n \right), \tag{36}$$

where k_B is the Boltzmann's constant, T is the temperature and χ is the Flory-Huggins parameter, which is a measure of the enthalpy of mixing. Note that Xue et al.[41,42] use a different approach. In these studies, the authors assume only the mixing of GAGs with solvent, while neglecting the collagen. Since we are considering GAGs and the collagen network as as a unique solid phase and we could not find any evidence that collagen does not mix with water, we have chosen the more general form (36).

As the interstitial fluid is well approximated by a dilute solution, the contribution ψ_4 reads [23,41,42]:

$$\psi_4 = k_B T \sum_{i=1}^{N} C_i \left(\ln \frac{C_i}{C_s} - 1 \right). \tag{37}$$

Finally, we need to specify the strain energy ψ_5. As mentioned in the introduction, the Standard Linear Solid (SLS), see Figure 1, is commonly used to describe soft material in the regime of small deformations. However, when account for large deformation, as in the case of swelling, soft material exhibit a non-linear behaviour [18]. For this reason we consider the model in Figure 6a, which is a generalization of the 1D SLS to 3D problems with non-linear elastic response.

The strain energy can thus be decomposed into the sum of the contributions from spring 1 and spring 2:

$$\psi_5 = \psi_{5.1}(\mathbb{F}) + \psi_{5.2}(\mathbb{F}_e). \tag{38}$$

As in [42], we consider the spring to be isotropic and hyper-elastic (Neo-Hookean) which are characterised by the following form of the free-energy:

$$\psi_{5.1}(\mathbb{F}) = \frac{G_1^A}{2} \left(\mathbb{F} : \mathbb{F} - 3 - 2 \ln J \right), \tag{39}$$

$$\psi_{5.2}(\mathbb{F}_e) = \frac{G_2^A}{2} \left(\mathbb{F}_e : \mathbb{F}_e - 3 - 2 \ln J_e \right), \tag{40}$$

where $G_{1,2}$ stands for the shear modulus associated with each spring, $J_e = \det \mathbb{F}_e$. As derived in [18], the hyper-elastic model (40) can be derived in the framework of statistical mechanics based on the microscopic properties of a polymer

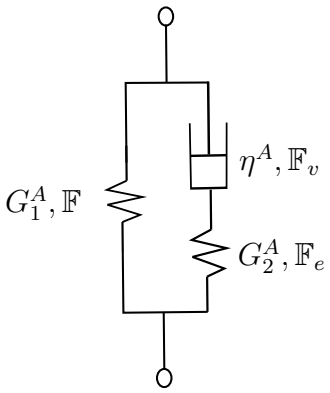

(a)

Element	**Constitutive Properties**	**Deformation**
spring 1	Isotropic Neo-Hookean spring	volumetric + deviatoric
spring 2	Isotropic Neo-Hookean spring	volumetric + deviatoric
dashpot	Isotropic Linear dashpot	deviatoric

(b)

Fig. 6: (a) Schematic representation of the non-linear rheological model for ECM; (b) Table summarizing the major properties of the model components.

network. This assumes the network to consist of Gaussian chains and affine deformation. Other thermodynamically consistent forms of the stretching energy have been proposed in the literature [5,6,14] using different network models.

4.5 Entropy Production σ.

Having specified how the system interacts with its environment, we can now discuss how it dissipates energy. As mentioned in Section (4.2), there are two contributions: transport (diffusion of solvent and solutes) and viscosity. The thermodynamic fluxes [7] associated with these two phenomena are $\mathbf{J}_m$, $m = s, 1, \ldots, N$, and $\mathbb{L}_v$. Consequently, using Equation (6), we obtain:

$$\sigma = \sum_m \zeta_m \cdot \mathbf{J}_m + \zeta_v : \mathbb{L}_v, \tag{41}$$

where ζs represent the thermodynamic forces associated with each flux. On the other hand, the rates $\Lambda = \left\{\dot{C}_s, \dot{C}_i, \dot{\mathbf{H}}, \dot{\mathbb{F}}\right\}$ describe the evolution of reversible process[8] and thus do not belong to the set of constitutive physical variables[9]. As discussed in detail in Appendix B, this implies that energy imbalance inequality (33) is linear in the variables Λ, so that the terms highlighted in blue in Equation (33) must be identically zero. This leads to the hold system of state

[7] See Section 3

[8] energy and entropy in reversible processes are state functions; consequently the state of the system does only depend on the value of the thermodynamic variables and not the rate at which they change.

[9] see Appendix B

equations (see Appendix B):

$$\mu_s = pv_s + \mu_s^0 + k_B T \left[\ln \frac{C_s v_s}{1 + C_s v_s} + \frac{1}{1 + C_s v_s} + \frac{\chi}{(1 + C_s v_s)^2} - \sum_i \frac{C_i}{C_s} \right], \tag{42}$$

$$\mu_i = \mu_i^0 + e\Phi z_i + kT \ln \frac{C_i}{C_s}, \tag{43}$$

$$-\epsilon J \nabla^2 \Phi = Q\,, \tag{44}$$

$$\mathbb{T} = -p\mathbb{I} + \frac{G_1^A}{1 + C_s v_s} (\mathbb{B} - \mathbb{I}) + \frac{G_2^A}{1 + C_s v_s} (\mathbb{B}_e - \mathbb{I}) + \underbrace{\epsilon \left[\frac{1}{2} |\nabla \Phi|^2 \mathbb{I} - \nabla \Phi \otimes \nabla \Phi \right]}_{\mathbb{T}^{Max}}, \tag{45}$$

where $\mathbb{T}^{max}$ is the component of the stress tensor due to the presence of the electric field. As discussed in Section 3, in the framework of linear non-equilibrium thermodynamics, when considering isothermal transformations, the second law of thermodynamics can be rewritten as Equations (9). Using the same argument as in Section 4.3, we can rewrite Equations (9) in differential form, and substituting Equations (42)-(45), we obtain:

$$\sigma = -\sum_m T^{-1} \nabla_0 \mu_m \cdot \mathbf{J}_m + T^{-1} \mathbb{M}_e : \mathbb{L}_v. \tag{46}$$

Equating Equation (46) and (41), it is natural to identify that the thermodynamics forces as:

$$\zeta_m = -\frac{1}{T} \nabla_0 \mu_m, \tag{47}$$

$$\zeta_v = \frac{1}{T} \mathrm{DEV}[\mathbb{M}_e] = \frac{G_2^A}{T} \mathrm{DEV}[\mathbb{C}_e]. \tag{48}$$

Assuming to be in a regime of linear non-equilibrium thermodynamics, we can use the identity (7) to linearly couple fluxes and forces. However, considering the symmetry constraint imposed by *Curie's law*[10] , there can be no coupling between fluxes and forces of a different tensorial nature. Consequently, we are left with the following force-flux relation:

$$\mathbb{L}_v = L_{vv} \zeta_v = \frac{L_{vv} G_2^A}{T} \mathrm{DEV}[\mathbb{C}_e], \tag{49}$$

$$\mathbf{J}_m = \sum_{k=s,1,\ldots,N} L_{mk} \zeta_k = - \sum_{k=s,1,\ldots,N} \frac{L_{mk}}{T} \nabla_0 \mu_k. \tag{50}$$

[10] Macroscopic causes can not have more elements of symmetry than the effect they cause [29]

As described in Appendix C, starting from Equations (47)-(50) and with common consideration from the theory of mixture, we can derive the following system of time dependent equations:

$$\partial_t C_s = \nabla_0 \cdot \left[K\mathbb{F}^{-1} \left(C_s \nabla \mu_s + \sum_i \frac{D_i}{D_i^0} C_i \nabla \mu_i \right) \right], \tag{51}$$

$$\partial_t C_i = \nabla_0 \cdot \left[\frac{D_i}{k_B T} C_i \mathbb{F}^{-1} \nabla \mu_i - \frac{D_i}{D_i^0} \frac{C_i}{C_s} \mathbf{J}_s \right], \tag{52}$$

$$\dot{\mathbb{B}}_e = \mathbb{L}\mathbb{B}_e + \mathbb{B}_e \mathbb{L}^T - \frac{1}{\tau_R} \mathbb{B}_e \mathrm{DEV}[\mathbb{B}_e]. \tag{53}$$

where the parameters (see the Glossary) are macroscopic phenomenological coefficients. To sum up, Table (1) lists the variables and corresponding governing equation for model A as well as model B, which we recall has been derived in Appendix D. In order to have a close solution, the proper boundary and initial conditions needs also to be assigned but these will be specified depending on the specific problem considered.

Variable	Model A	Model B	Equation Type
Solvent Concentration	C_s (56)		Governing
Chemical Potential of the solvent	μ_s (42)		State
Ionic Concentrations	C_i (57)		Governing
Chemical Potential of the ions	μ_i (43)		State
Local Volumetric Change	J (11)		State
Cauchy Stress Tensor	$\mathbb{T}$ (15)		State
Deformation Gradient	$\mathbb{F}$ (A)	$\mathbb{F}$ (B)	State
Pore Pressure	p (45)	p 124)	State
Left-Cauchy Tensor for spring 2	$\mathbb{B}_e$ (53)	$\bar{\mathbb{B}}_e$ (128)	Governing
Viscous Velocity Gradient Tensor	$\mathbb{L}_v$ (98)	$\bar{\mathbb{L}}_v$ (125)	Governing
Electric Field	Φ (44)		State
Local charge	Q (19)		State

Table 1: List of Variables involved in the problem, with reference to the corresponding governing equations. We denote by state equation, the constitutive equations that defines a variable in terms of the state of the system. On the other hand, governing equations explicitly contain the time variable t as they describe the evolution of a non-reversible process.

5 Summary of the Evolution Equation.

Having derived the full model for both decomposition of $\mathbb{F}$, we discuss more in details their physical interpretation, with particular interest at the governing equations. We first rewrite the solvent chemical potential, Equation (43), as:

$$\mu_s = \mu_s^0 + k_B T \left(\frac{p v_s}{k_B T} + \Pi_{osm} - \sum_i \frac{C_i}{C_s} \right), \tag{54}$$

$$\Pi_{osm} = \ln \frac{C_s v_s}{1 + C_s v_s} + \frac{1}{1 + C_s v_s} + \frac{\chi}{(1 + C_s v_s)^2}, \tag{55}$$

where p represents the pore pressure and Π_{osm} is the osmotic pressure of the solution. If we now substitute into Equation (51) the chemical potentials (54)-(43), this yields to:

$$\begin{aligned} \partial_t C_s = \nabla_0 \cdot \Bigg\{ K \mathbb{F}^{-1} \Bigg[& C_s v_s \nabla p + \sum_i \frac{D_i}{D_i^0} C_i e z_i \nabla \Phi. + k_B T \left(C_s \nabla \Pi_{osm} + \right. \\ & \left. \sum_i \left(1 - \frac{D_i C_i}{D_i^0 C_s} \right) \nabla C_s - \sum_i \left(1 - \frac{D_i}{D_i^0} \right) \nabla C_i \right) \Bigg] \Bigg\}. \end{aligned} \tag{56}$$

The above equation shows that the solvent transport is driven by the hydrostatic pressure gradient, the osmotic pressure gradient (blue-green term in Equation (56)) and the electric potential gradient[11]. If we consider the limit $v_s C_s \to \infty$, Equation (56) reduces to Darcy's law for the flow in a porous media. The model for polyelectrolytes proposed by Hong [23] corresponds instead to the limit $D_i^0 \to \infty$, where mobile species can move freely in pure solution and the friction is due only to relative motion with the solid phase.

Similarly we can rewrite Equation (52) as:

$$\partial_t C_i = \nabla_0 \cdot \left[D_i \mathbb{F}^{-1} \left(\underbrace{\nabla C_i}_{\text{diffusion}} + \underbrace{\frac{e C_i z_i}{k_B T} \nabla \Phi}_{\text{electric}} \right) - \underbrace{\frac{D_i C_i}{C_s} \mathbb{F}^{-1} \nabla C_s}_{\text{osmotic pressure}} - \underbrace{\frac{D_i C_i}{D_i^0 C_s} \mathbf{J}_s}_{\text{advection}} \right]. \tag{57}$$

In the case of ions, the driving forces of transport are the diffusion of ions, the electric field, the osmotic pressure due to the mixing with the solvent and the advection term (due to the relative movement of ions with respect to the solvent). Again in the limit $D_i^0 \to \infty$, we recover the well-known model proposed by Hong [23] for polyelectrolytes. In the dilute limit, i.e. when the concentration of ions is much smaller than the solvent concentration $C_i << C_s$, we can drop both the osmotic and advection term so as to recover the well-known Nernst-Planck equation [23, see Equation (6.67)].

As mentioned in the introduction, we are particularly interested in the viscoelastic contribution to the system kinetics. Even though in the transport Equation (56)-(57) there is no direct reference to it, the transport is indirectly coupled

[11] equivalent to the electric field.

to the poro-relaxation through the pressure gradient. Taking the divergence of Equation (45) and using the conservation of momentum (15), we can identify different components of the pressure gradient:

$$\nabla p = \nabla \cdot \mathbb{T}^{Max} + G_1^A \underbrace{\nabla \cdot \left[\frac{\mathbb{B}-\mathbb{I}}{1+v_s C_s}\right]}_{\substack{\text{swelling} \\ \text{+ deviatoric} \\ \text{deformation}}} + G_2^A \underbrace{\nabla \cdot \left[\frac{\mathbb{B}_e-\mathbb{I}}{1+v_s C_s}\right]}_{\substack{\text{swelling} \\ \text{+ deviatoric} \\ \text{deformation} \\ \text{+ viscous relaxation}}} . \tag{58}$$

Unlike the standard Neo-Hookean model for polyelectrolytes, we have an additional term highlighted in red, which accounts for the energy stored in the second spring of model A. Its time evolution, as determined by Equation (53), is driven by both the macroscopic (both volumetric and deviatoric) deformation and the relaxation dynamics which captures the viscous nature of the solid phase:

$$\dot{\mathbb{B}}_e = \underbrace{\mathbb{L}\mathbb{B}_e + \mathbb{B}_e\mathbb{L}^T}_{\substack{\text{swelling} \\ \text{+ deviatoric} \\ \text{deformation}}} - \underbrace{\frac{1}{\tau_R}\mathbb{B}_e \text{DEV}[\mathbb{B}_e]}_{\substack{\text{viscous} \\ \text{relaxation}}} . \tag{59}$$

Despite the introduction of non-linearities, there is an apparent analogy between the above equation and the ODE describing the standard linear solid, see Equation (1) in the Introduction. The term $\dot{\epsilon} \leftrightarrow \mathbb{L}$ is related to the strain experienced by spring 1, while $\epsilon_e \leftrightarrow \mathbb{B}_e$ is the variable describing the strain on the string in the Maxwell branch. In the limit $\tau_R \to \infty$, we have that $\mathbb{B}_e \equiv \mathbb{B}$. We thus recover the standard Neo-Hookean hyper-elastic model for hydrogels with shear modulus given by $G_1^A + G_2^A$. Similar result are obtained for model B. The governing equation of model B is equivalent to (59), except that the relaxation is now not influenced by volumetric deformations:

$$\dot{\bar{\mathbb{B}}}_e = \underbrace{\bar{\mathbb{L}}\bar{\mathbb{B}}_e + \bar{\mathbb{B}}_e\bar{\mathbb{L}}^T}_{\substack{\text{deviatoric} \\ \text{deformation}}} - \underbrace{\frac{1}{\tau_R}\bar{\mathbb{B}}_e \text{DEV}[\bar{\mathbb{B}}_e]}_{\substack{\text{viscous} \\ \text{relaxation}}} . \tag{60}$$

Looking instead at the pressure gradient, we see that the volumetric and deviatoric contribution are now decoupled:

$$\begin{aligned} \nabla p = \nabla \cdot \mathbb{T}^{Max} + G_1^B \underbrace{\nabla \cdot \left[\frac{\text{DEV}[\bar{\mathbb{B}}]}{1+v_s C_s}\right]}_{\substack{\text{+ deviatoric} \\ \text{deformation}}} + G_{vol} \underbrace{\nabla\left(\frac{J^{2/3}-1}{J}\right)}_{swelling} \\ + G_2^B \underbrace{\nabla \cdot \left[\frac{\text{DEV}[\bar{\mathbb{B}}_e]}{1+v_s C_s}\right]}_{\substack{\text{deviatoric} \\ \text{deformation} \\ \text{+ viscous relaxation}}} . \end{aligned} \tag{61}$$

The two models are equivalent when $\mathbb{F}$ is iso-volumentric, i.e. $\det \mathbb{F} = 1$. In the case of purely volumetric deformation, i.e. $\mathbb{F} = \mathbb{F}_{vol} = J^{1/3}\mathbb{I}$, we have instead that the two models are equivalent given that $G_{vol} \equiv G_A + G_B$. However, as we will be discussing in the next section, differences emerge when the deformation gradient has both an hydrostatic and a non-zero deviatoric component.

6 Elasticity: Equilibrium Behaviour.

As common in the literature of polyelectrolytes modelling, we study our models in two different settings: free and compressed swelling. Despite considering equilibrium conditions, these experiments allow us to estimate a subset of the many parameter in the model. As we will see also in this simplified setting where the dynamics is neglected important differences emerges between the two model presented, which result in relevant quantitative discrepancy in the predictions. Our aim is thus to understand which experiments are necessary in order the most appropriate model to describe a soft material.

Throughout this section, unless specified otherwise, we will be using the parameters listed in Table 3 in Appendix E.

6.1 Unconstrained Free Swelling.

First of all, we study the unconstrained free swelling of a cuboid slice of ECM when immersed in a bath of interstitial fluid. For simplicity we consider that the latter contains only two species of free ions: a positive C_+ and a negative C_- one. We further assume the bath to be well-mixed and stress-free with both pressure and electric potential identically zero. Given $2c_0$ to be the total concentration of free ions in the neutral bath, c_0 denotes the concentration of each ionic species. As the system evolves, proper boundary conditions require the continuity of chemical potentials and stresses across the boundary:

$$[\mu_s]^+_- = [\mu_+]^+_- = [\mu_-]^+_- = 0, \quad [\mathbf{n}\mathbb{T}\mathbf{n}]^+_- = 0. \tag{62}$$

with $[\cdot]^+_-$ denoting the change in the value of a variable across the tissue boundary.

An additional boundary condition is necessary due to the second-order derivatives in Φ in Equation (44). Unlike the other variables, the electrostatic potential in the ECM rapidly change near the boundary. This creates a thin charged interface [43]. Since its thickness is negligible compared to the size of the ECM, we consider Φ to be discontinuous at the interface, while the associated stress $\mathbb{T}^{Max}$ vanishes on the boundary:

$$\nabla\Phi \cdot \mathbf{n}|_- = 0. \tag{63}$$

As the tissue is assumed to be isotropic and homogeneous, the deformation gradient tensor $\mathbb{F}$ reads:

$$\mathbb{F} = \lambda\mathbb{I}, \tag{64}$$

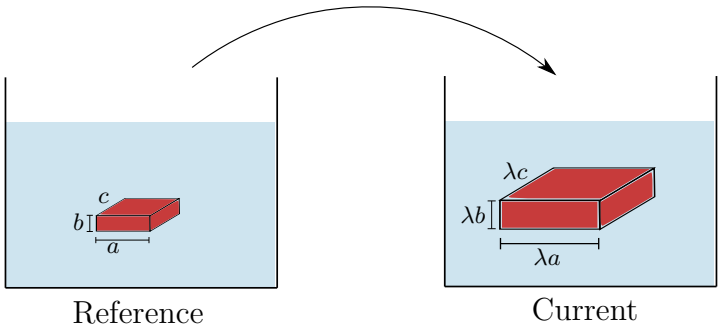

Fig. 7: Schematic representation of a free swelling. Since we are considering an isotropic mixture, the ECM maintains its shape while all dimension are stretched of the same amount λ. So that the relative volume change is $\delta V = \lambda^3 - 1$.

with the stretch $\lambda = (1 + C_s v_s)^{1/3}$. Following [16], the equilibrium state is characterized by the following conditions:

1. chemical potentials of solvent and solutes are homogeneous and equal in the bath and in the tissue:

$$\mu_s = \mu_s^{ext} = \mu_s^0 - vkT \sum_i c_0^i, \tag{65}$$

$$\mu_i = \mu_i^{ext} = \mu_i^0 + kT \ln(v_s c_0^i). \tag{66}$$

2. Φ is constant in the tissue so that $\nabla \Phi \equiv \mathbf{0}$ in the interior of the domain.
3. The stress tensor $\mathbb{T}$ is constant and equal to the value in the bath:

$$\mathbb{T} = 0. \tag{67}$$

As shown in Appendix F, imposing the equilibrium conditions, we obtain that for both models the equilibrium stretch λ is implicitly defined by the following algebraic equation:

$$F(\lambda) = \frac{\lambda^3 + \chi}{\lambda^6} + \frac{p v_s}{k_B T} + \ln \frac{\lambda^3 - 1}{\lambda^3} + 2 c_0 v_s - \sqrt{\left(\frac{z_f C_f v_s}{\lambda^3 - 1}\right)^2 + 4 v_s^2 c_0^2} = 0, \tag{68}$$

where the pressure p is defined depending on the model considered as:

$$p = \begin{cases} \dfrac{G_{eq}^A}{\lambda^3}(\lambda^2 - 1) & \text{MODEL A,} \\ \dfrac{G_{vol}^B}{\lambda^3}(\lambda^2 - 1) & \text{MODEL B,} \end{cases} \tag{69}$$

with $G_{eq}^A = G_1^A + G_2^A$. In this case, both models reduce to the standard hyperelastic model for polyelectrolytes proposed by Hong [23]. As this has been previously discussed in the literature, we only present its most important features. As illustrated in Figure 8, the ion concentration c_0 affects the degree of swelling. However it is the mixing parameter χ which defined the tissue phase. This can either be in a highly swollen or a collapsed phase, where the latter is characterised by low absorption of fluid [43].

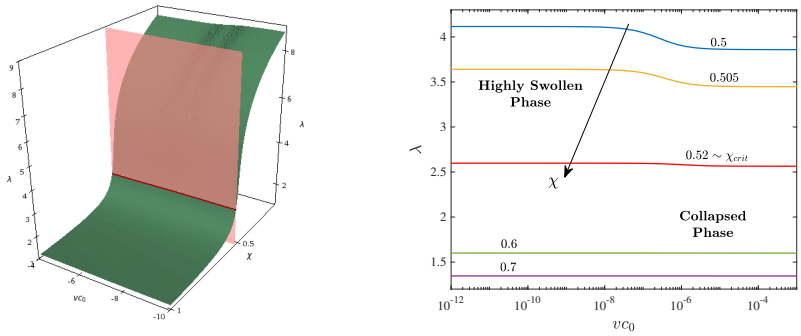

(a) (b)

Fig. 8: Free Swelling: (a) Manifold implicitly defined by Equation (68) where $G^A_{eq} = 10^3$ is fixed, while c_0 and χ are varied. On the vertical axis is λ as defined by (64). The red plane corresponds to $\chi = \chi_{crit}$ and splits the parameter space into the region of high swelling and collapse for the material [43]. (b) Section of the manifold in Figure (a) for different values of χ.

7 Confined Compression Test.

A second common test conducted on soft material is confined compression. As illustrated in Figure 9, a porous plate is used so that the fluid is free to flow and the chemical equilibrium with the external bath is restored after the transient relaxation phase. After gradual compression of the tissue, the system is allowed to relax while the strain ϵ is maintained constant [34]. We here interested in the equilibrium, i.e. relaxed, behaviour of the sample, which is described by a stress-strain curve (see Figure 10a as an example).

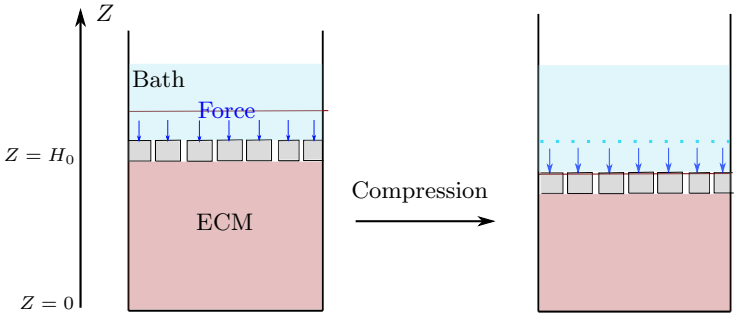

Fig. 9: Schematic representation of a compression test with a porous piston. A deformation is imposed in the Z direction and the force necessary to maintain the deformation is recorded.

As we consider a swollen slice of tissue compressed in the Z direction, the deformation $\mathbb{F}$ from the dry to the current state has the form:

$$\mathbb{F} = J_0^{1/3} \begin{bmatrix} 1 & 0 & 0 \\ 0 & 1 & 0 \\ 0 & 0 & \lambda_1 \end{bmatrix}, \tag{70}$$

where $\lambda_1 = 1 - \epsilon$ and J_0 defines the initial swollen state.

As the problem is one-dimensional, we can reduce the number of unknowns. We define $u = \mathbf{u} \cdot \mathbf{e}_Z$, $T_{zz} = \mathbf{e}_Z \mathbb{T} \mathbf{e}_Z$ and $J_m = \mathbf{J}_m \cdot \mathbf{e}_Z$, the component of the displacement, deformation tensor and fluxes in the Z direction. Assuming the slice to have an initial height H_0, proper boundary conditions need to be assigned at the two edges $Z = 0$ and $Z = H_0$:

$$[\mu_s]_-^+ = [\mu_+]_-^+ = [\mu_-]_-^+ = 0, \quad [T_{zz}]_-^+ = 0, \qquad Z = H_0\,, \tag{71}$$

$$J_m = u = 0, \qquad Z = 0\,, \tag{72}$$

$$\frac{\mathrm{d}\Phi}{\mathrm{d}Z} = 0 \qquad Z = 0, H_0\,. \tag{73}$$

At equilibrium, the conditions 1 and 2 listed in Section 6.1 still hold. On the other hand, due to the external force $\mathbf{F} = -F_z \mathbf{e}_z$ which is exerted on the plate of area A, condition 3 now reads:

$$T_{zz} = \sigma = -\frac{F_z}{A}. \tag{74}$$

7.1 Model Comparison.

Starting from model A, given the symmetries of the problem, $\mathbb{B}_e$ is a diagonal matrix of the form:

$$\mathbb{B}_e = \begin{bmatrix} b & 0 & 0 \\ 0 & b & 0 \\ 0 & 0 & b_1 \end{bmatrix}. \tag{75}$$

If we now study the fixed point of Equation (53), we obtain that $b = b_1 = J_0^{2/3} \lambda_1^{2/3}$ as $\det \mathbb{B}_e = (\det \mathbb{F})^2$.

Focusing on model B instead, the tensors $\bar{\mathbb{B}}$ and $\bar{\mathbb{B}}_e$ are now of the form:

$$\bar{\mathbb{B}} = \begin{bmatrix} \lambda_1^{-2/3} & 0 & 0 \\ 0 & \lambda_1^{-2/3} & 0 \\ 0 & 0 & \lambda_1^{4/3} \end{bmatrix}, \qquad \bar{\mathbb{B}}_e = \begin{bmatrix} \bar{b} & 0 & 0 \\ 0 & \bar{b} & 0 \\ 0 & 0 & \bar{b}_1 \end{bmatrix}, \tag{76}$$

with the $\bar{b} = \bar{b}_1 = 1$ at equilibrium so that the spring 2 does not contribute to the stress. Substituting the equilibrium conditions into the state equations for

the two models (see Table 1) yields to:

$$p = \begin{cases} -\sigma + \dfrac{G_1^A}{J_0\lambda_1}(J_0^{2/3}\lambda_1^2 - 1) + \dfrac{G_2^A}{J_0\lambda_1}(J_0^{2/3}\lambda_1^{2/3} - 1) & \text{MODEL A,} \\ -\sigma + \dfrac{G_{vol}}{J_0\lambda_1}(J_0^{2/3}\lambda_1^{2/3} - 1) + \dfrac{2G_1^B}{3J_0\lambda_1^{5/3}}(\lambda_1^2 - 1) & \text{MODEL B,} \end{cases} \tag{77}$$

$$\frac{\sigma v_s}{k_B T} = \frac{J_0\lambda_1 + \chi}{J_0^2\lambda_1^2} + \frac{p v_s}{k_B T} + \ln\frac{J_0\lambda_1 - 1}{J_0\lambda_1} + 2c_0 v_s - \sqrt{\left(\frac{z_f C_f v_s}{J_0\lambda_1 - 1}\right)^2 + 4v_s^2 c_0^2}. \tag{78}$$

Unlike for unconstrained swelling, we note that model A and B are now substantially different, as there is no choice of parameter values for which the two are equivalent for any value of λ_1.

Following the work of Xue et al [42], we test our models on the data collected by Netti et al. [34] on HSTS 26T sarcoma slices. Despite our model being built to describe decellularized ECM, cells can be included in the model simply as part of the solid phase [42]. As we are interested in the tissue scale, this is a good approximation. However, as suggested also by Xue et al.[42], more accurate models also incorporate the cellular activities. However, this goes beyond the purpose of our study.

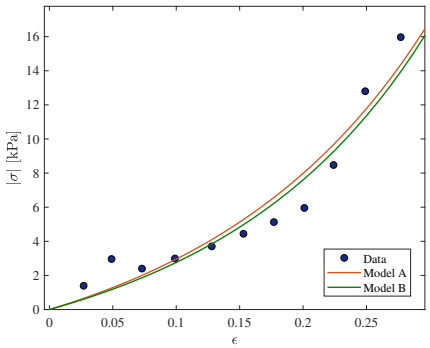

(a) Fitted Model

Model A		Model B	
χ	0.498	χ	0.524
G_1^A	18.9 kPa	G_{vol}	75 Pa
G_2^A	5.3 Pa	G_1^B	55.1 kPa
J_0	20.7	J_0	14.8

(b) Estimated Parameters

Fig. 10: Comparison of the two models in fitting real experimental data from [34].

Together with the stress-strain curve from the compression test, Netti et al. measure also the tissue composition, so that C_f is known (see Table 3). The other parameters listed in Table 3 have been taken from the literature. Consequently the set of unknown parameters is $\{\chi, G_1^A, G_2^A\}$ and $\{\chi, G_{vol}, G_1^B\}$ for models A and B respectively. These are estimated fitting Equation (78) to the data,

using the `fmincon` function in MATLAB, which implements the non-linear least squares method[12].

As shown in Figure 10a, both models are able to capture the qualitative behaviour of the data. However they largely disagree in their quantitative predictions, see Table 10b. Let us for example compute the initial pressures in the tissue slice, i.e. p at $\lambda_1 = 1$:

$$p_A = \frac{G_1^A + G_2^A}{J_0}(J_0^{2/3} - 1) = \frac{24.2 \text{ kPa}}{20.7}(20.7^{2/3} - 1) = 7.64 \text{ kPa}, \tag{79}$$

$$p_B = \frac{G_{vol}}{J_0}(J_0^{2/3} - 1) = \frac{0.075 \text{ kPa}}{14.8}(14.8^{2/3} - 1) = 25.5 \text{ Pa}, \tag{80}$$

then the two differ of several order of magnitude. Consequently, the models give a completely different estimation of the pressure cells in the tissue are exposed to. As hydrostatic pressure affect cells behaviour [11], based on which model is considered, we could end up with completely different conclusion on the mechano-sensitivity of cells.

Looking at the Table 10b, we note that $G_{vol} \neq G_1^A + G_2^A$, so that, the two estimated models would disagree also in the case of free-swelling. Based on the result from Section 6.1, we propose that a two-step protocols which combines free-swelling and compression test can be more informative to identify the material properties. To reproduce this setting *in silico*, we compare again models A and B simulating a compression experiment. This time however we assume that the parameters χ and $G_{vol} = G_{eq}^A$ are fixed, as if they have been previously estimated by unconstrained swelling experiment. If we now take the difference between the compression stress predicted by Equation (78) for the two models, i.e. $\delta\sigma = \sigma_B - \sigma_A$, we obtain:

$$\delta\sigma = \frac{2G_1^B}{3}\frac{\lambda_1^2 - 1}{J_0\lambda_1^{5/3}} - \frac{G_1^A}{J_0^{1/3}}(\lambda_1 - \lambda_1^{-1/3}). \tag{81}$$

For the purpose of our analysis, we impose the two models to agree at the second order in the regime of small deformation. This translates in the conditions $\lambda_1 \to 1$:

$$\delta\sigma|_{\lambda_1=1} = 0 \qquad \left.\frac{\mathrm{d}\delta\sigma}{\mathrm{d}\lambda_1}\right|_{\lambda_1=1} = 0 \quad \Rightarrow \quad G_1^B = J_0^{2/3}G_1^A. \tag{82}$$

Under such conditions we can rewrite Equation (81) as:

$$\delta\sigma(\lambda_1; G_1^A, J_0) = \frac{G_1^A}{J_0^{1/3}\lambda_1^{5/3}}\left(\frac{2}{3}\lambda_1^2 - \frac{2}{3} - \lambda_1^{5/3} + \lambda_1^{4/3}\right), \tag{83}$$

where J_0 is defined by Equation (68). As shown in Figure 11, $\delta\sigma$ is an increasing function of ϵ as the two model appear to diverge exponentially as $\epsilon \to 0$.

[12] the result as been optimized starting from different initial condition, so to explore a larger part of the parameter space

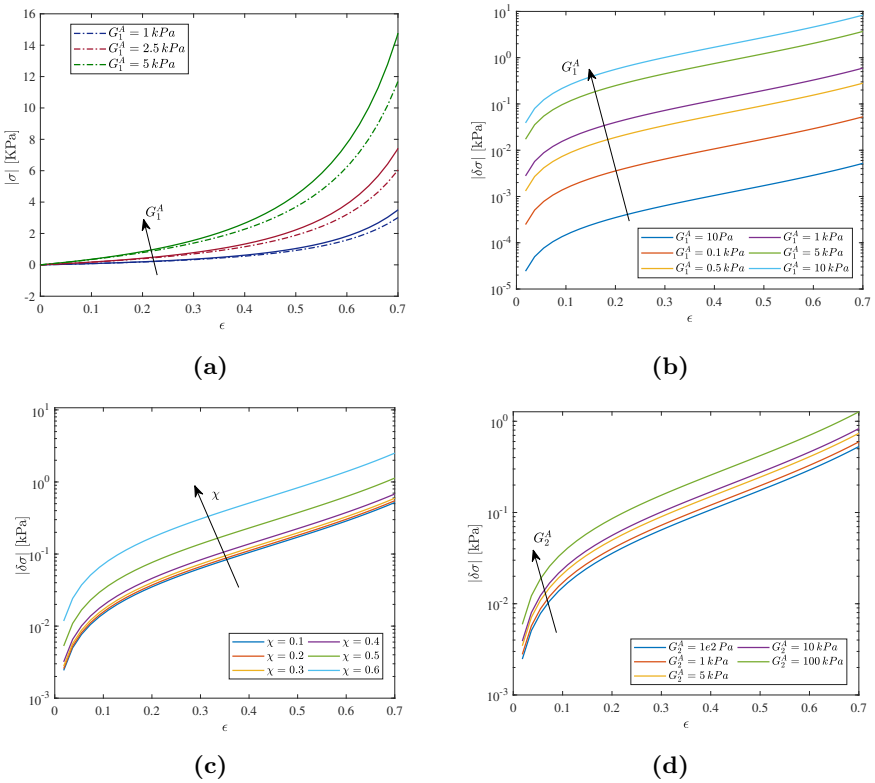

Fig. 11: Sensitivity Analysis. As expected the mismatch between the two models grows with the strain: (a) Comparison of stress-strain curve predicted by model A (dotted line) and model B (full line) for different values of the parameter G_1^A; (b) as G_1^A increases so does the discrepancy $\delta\sigma$; (c) $\delta\sigma$ is also particularly sensitive to changes in the mixing parameter χ, in particular we see that there is a relevant jump when the ECM is in the *collapsed* phase; (d) on the other hand, only large changes in G_2^A have a relevant impact on $\delta\sigma$.

Consequently, in the large-deformation regime we should be able to distinguish between the two models. Let us consider the case in which χ and G_{vol} are estimated by free-swelling experiment as in Figure (10b). Using Equation (82) and the condition $G_{vol} = G_{eq}^A$, we would have that $G_2^A < 0$, which is not physically admissible. This is to highlight how, having information about free and constraint swelling can be informative in identifying the proper model.

We could not find data from the literature for both swelling and compression tests on tissues, so that we can not yet conclude whether both, one or none of the models effectively describe soft tissue. This will require further experimental testing. With this aim, we have also performed a sensitivity analysis on the model parameters. As illustrated in Figure (11), χ and G_1^A are the parameters that have the more impact on $\delta\sigma$. While G_1^A depends only on the properties of the material, χ can be tuned by changing the temperature T so to optimise the experimental condition.

8 Conclusion and Further Work.

Our work has been motivated by the recent evidence of the visco-elastic behaviour of soft tissue and in particular of the extracellular matrix (ECM). Experimental studies have shown that in tumours, the ECM undergoes stiffening [42], which relates to poor efficacy of chemotherapy and positively correlates with the formation of metastasis. On the other hand, little is known on the effect of visco-elasticity on the cell micro-environment and the consequence this might have on healthy and damaged tissues. As synthetic ECM with tunable visco-elasticity are now produced, there has been a growing interest in investigating also this aspect of the cell microenvironment [11].

We have developed a thermodynamically consistent poro-visco-elastic model for polyelectrolyte gels, and more specifically for the extracellular matrix. To the best of our knowledge, this is the first time visco-elasticity is introduced in the framework of linear non-equilibrium thermodynamics to describe polyelectrolytes, which are usually modelled as purely hyper-elastic and porous materials. Unlike in poro-elastic models, the introduction of viscous (or also plastic) effects requires specification of a multiplicative decomposition of the deformation tensor $\mathbb{F}$, depending on how viscous and elastic components of the deformation couple.

Starting from two of the most common decompositions in the framework of large deformations, we have investigated how the two reflect on the behaviours of a material. As standard in the literature of hydrogels and soft tissues [9,16,42], we test our models on two different settings: free swelling and confined compression tests. Our analysis shows that while the two models agree in the free-swelling, they differ in the case of compression test. As shown in Section 7.1 using experimental data from previous literature [34], the two models have similar qualitative behaviour, but differ by several orders of magnitude in their quantitative predictions. As the compression test alone is not sufficient in model validation and selection, we propose a two step protocol which includes both free-swelling and constraint compression experiments. The first natural extension of this work is thus performing such experiments on ECM samples. Having selected the most appropriate model, the interplay of viscosity, pressure and diffusion phenomena can be investigated by analysing the dynamics of the model and comparing it with temporal data from non-static experiments. In particular numerical simulation of in silico together with *in vitro* AFM experiments can be used to better understand how measurement at the micro-scale relates to the tissue dynamics so as to get new insights into the micro-environment cell experience.

A Glossary of Variables and Parameters in the Model.

ψ	Helmholtz free energy per unit volume in the initial configuration,
$\mathbf{u}$	Displacement vector,
$\mathbb{F}$	Deformation gradient tensor $\mathbb{F} = \mathbb{I} - \nabla_0 \mathbf{u}$,
$\mathbb{C}$	Right Cauchy-Green Tensor $\mathbb{C} = \mathbb{F}^T\mathbb{F}$,
$\mathbb{B}$	Left Cauchy-Green Tensor $\mathbb{B} = \mathbb{F}\mathbb{F}^T$,
$\mathbb{L}$	Velocity Gradient Tensor $\mathbb{L} = \dot{\mathbb{F}}\mathbb{F}^{-1}$,
$\mathbf{H}$	Nominal Electric Displacement,
$\mathbf{E}$	Nominal Electric Field,
Q	Local net charge considering solid and ionic phases,
Φ	Electric Potential,
e	Elementary Charge,
J	Determinant of the deformation gradient tensor $J = \det \mathbb{F}$,
C_f	Concentration of fixed charges in the network,
z_f	Charge of a GAG chain,
v_m	Characteristic molecular volume of the species m,
η^A	Viscosity of the collagen network in model A,
G_1^A	Shear modulus related to spring 1 in model A,
G_2^A	Shear modulus related to spring 2 in model A,
G_{vol}	Shear modulus for the volumetric spring in model B,
G_1^B	Shear modulus related to spring 1 in model B
G_2^B	Shear modulus related to spring 2 in model B
η^B	Viscosity of the collagen network in model A,
τ_R	Viscous relaxation time of the collagen network,
D_i^0	Diffusion coefficient for the i-th solute species when in pure solvent (interstitial fluid),
D_i	Diffusion coefficient for the i-th solute species in ECM,
K	Hydraulic permeability of the ECM to the interstitial fluid (solvent+solute),
k	Hydraulic permeability to pure solvent (water),
$\mathbb{S}$	First Piola-Kirchoff tensor,
$\mathbb{T}$	Cauchy stress tensor, $\mathbb{T} = J^{-1}\mathbb{S}\mathbb{F}^T$,
p	Hydrostatic pressure,
$\mathbb{T}^{Max}$	Maxwell stress due to the electric displacement,
$\mathbb{M}_e$	Mandel stress,
k_B	Boltzmann constant,
T	Absolute Temperature,
$\mathbf{n}$	Normal Vector,
$\mathbf{e}_{x,y,z}$	Canonical Basis in Cartesian Coordinates,
$\mathrm{DEV}\,[\cdot]$	Deviatoric part of the tensor $\mathrm{DEV}\,[\cdot] = \cdot - 1/3\,\mathrm{tr}(\cdot)$,
$[\cdot]^+_-$	Change in the value of a variable across the tissue boundary.

B State Equation for Model A.

Thermodynamics theory describe the state of a system in terms of primitive physical quantities [21]. As shown in Table (2), this can be divided into independent and dependent variables. While the fist are the variables of the model, the second are uniquely defined as a function of the independent variables, i.e. a *state equation*. This are of the form:

$$\mathbf{E} = \mathbf{E}(C_m, \mathbb{F}, \mathbf{H}, \mathbb{F}_e, \mu_m, \mathbb{M}_e, \nabla\mu_m), \tag{84}$$

where $\mathbf{E}$ can be replaced by any dependent variable. The split between dependent and independent variables is usually arbitrary, but it comes natural when looking at the energy inequality.

Independent		Dependent
Reversible	Irreversible	
$C_m,\ \mathbb{F},\ \mathbf{H}, \mathbb{F}_e$	$\mu_m, \mathbb{M}_e, \nabla\mu_m$	$\mathbf{E}, \mathbb{S}, p$ $\Phi, \mathbf{J}_m, \mathbb{L}_v$

Table 2: Constitutive Variables.

When considering independent variables, this can be further split into the one that describe a reversible and an irreversible process. Depending on the system properties the latter can be associated with thermodynamic force (see Section 3). Note that, the rate of change, i.e. time derivative, of reversible variables does not appear in the list of constitutive variables. This is because the state of a system during a reversible (ideal) transformation depend only on the current value of the thermodynamic variable and not at the rate at which they change[27]. This has two main consequence: the value of the rate variables Γ (see Glossary or Section 4.5) can be chosen arbitrarily by setting the proper experimental condition, and the energy imbalance inequality (33) is linear in this terms. Consequently, we have that in order for the energy imbalance inequality to hold for any arbitrary choice of Γ, the term in the blue brackets of Equation (33) must be identically zero:

$$\mu = \frac{\partial\psi}{\partial C} + pv_s, \tag{85}$$

$$\mathbf{E} = \frac{\partial\psi}{\partial\mathbf{H}}, \tag{86}$$

$$\mu_i = e\Phi z_i + \frac{\partial\psi}{\partial C_i}, \tag{87}$$

$$\mathbb{S} = \frac{\partial\psi}{\partial\mathbb{F}} + \frac{\partial\psi}{\partial\mathbb{F}_e}\mathbb{F}_v^{-T} - pJ\mathbb{F}^{-T}. \tag{88}$$

Using the explicit form of the free-energy ψ discussed in Section (4.4) and the definition of the stress tensor (16), we obtain:

$$\begin{aligned}\mu_s = pv_s + \mu_s^0 + kT \Bigg[\ln \frac{C_s v_s}{1 + C_s v_s} + \frac{1}{1 + C_s v_s} \\ + \frac{\chi}{(1 + C_s v)^2} - \sum_i \frac{C_i}{C_s} \Bigg],\end{aligned} \tag{89}$$

$$\mathbf{E} = \frac{1}{\epsilon J} \mathbb{F}^T \mathbb{F}\, \mathbf{H}, \tag{90}$$

$$\mu_i = \mu_i^0 + e\Phi z_i + kT \ln \frac{C_i}{C_s}, \tag{91}$$

$$\begin{aligned}\mathbb{T} = -p\mathbb{I} + \frac{G_1^A}{1 + C_s v_s} (\mathbb{B} - \mathbb{I}) + \frac{G_2^A}{1 + C_s v_s} (\mathbb{B}_e - \mathbb{I}) \\ - \frac{1}{\epsilon} \left(\frac{1}{2}\, \mathbf{h} \cdot \mathbf{h} \mathbb{I} - \mathbf{h} \otimes \mathbf{h} \right).\end{aligned} \tag{92}$$

Rewriting Equation (90) in terms of variables in the current configuration and using the definition of the electrical potential, Equation (17), we obtain:

$$\mathbf{h} = \epsilon \mathbf{e} = -\epsilon \nabla \Phi. \tag{93}$$

Substituting the above equation into Gauss law (18) and (92), we can rewrite the System (89)-(92) as:

$$\begin{aligned}\mu_s = pv_s + \mu_s^0 + k_B T \Bigg[\ln \frac{C_s v_s}{1 + C_s v_s} + \frac{1}{1 + C_s v_s} \\ + \frac{\chi}{(1 + C_s v_s)^2} - \sum_i \frac{C_i}{C_s} \Bigg],\end{aligned} \tag{94}$$

$$\mu_i = \mu_i^0 + e\Phi z_i + kT \ln \frac{C_i}{C_s}, \tag{95}$$

$$-\epsilon J \nabla^2 \Phi = Q\,, \tag{96}$$

$$\begin{aligned}\mathbb{T} = -p\mathbb{I} + \frac{G_1^A}{1 + C_s v_s} (\mathbb{B} - \mathbb{I}) + \frac{G_2^A}{1 + C_s v_s} (\mathbb{B}_e - \mathbb{I}) \\ + \epsilon \left[\frac{1}{2} |\nabla \Phi|^2 \mathbb{I} - \nabla \Phi \otimes \nabla \Phi \right],\end{aligned} \tag{97}$$

C Energy Dissipation.

In this section, we expose the details of the derivation of the governing equations (51)-(53) presented in Section (4.5).

Combining Equations (47) and (49), we can characterise the viscous flow by the following relation:

$$\mathbb{L}_v = \frac{L_{vv}}{T}\text{DEV}[\mathbb{M}_e] = \frac{L_{vv}}{T}\text{DEV}\left[\mathbb{F}_e^T\frac{\partial\psi}{\partial\mathbb{F}_e}\right] = \frac{G_2^A}{\eta^A}\text{DEV}\left[\mathbb{C}_e\right], \tag{98}$$

where η^A represents the viscosity of the material. If we denote by τ_R the time-scale of the viscous relaxation this is define as:

$$\tau_R = \frac{\eta^A}{2G_2^A}. \tag{99}$$

If we now consider the left elastic Cauchy Green tensor $\mathbb{B}_e = \mathbb{F}_e\mathbb{F}_e^T$, we can relate its time derivative to $\mathbb{L}_v$ and $\mathbb{L} = \dot{\mathbb{F}}\mathbb{F}^{-1}$:

$$\begin{aligned}\dot{\mathbb{B}}_e &= \mathbb{L}\mathbb{B}_e + \mathbb{B}_e\mathbb{L}^T - 2\mathbb{F}_e d_v\mathbb{F}_e^T\\ &= \mathbb{L}\mathbb{B}_e + \mathbb{B}_e\mathbb{L}^T - \frac{1}{\tau_R}\mathbb{F}_e\left[\mathbb{C}_e - \frac{1}{3}tr(\mathbb{B}_e)\mathbb{I}\right]\mathbb{F}_e^T\\ &= \mathbb{L}\mathbb{B}_e + \mathbb{B}_e\mathbb{L}^T - \frac{1}{\tau_R}\mathbb{B}_e\underbrace{\left[\mathbb{B}_e - \frac{1}{3}tr(\mathbb{B}_e)\mathbb{I}\right]}_{\text{DEV}[\mathbb{B}_e]}.\end{aligned} \tag{100}$$

For what concern the dissipation due to transport phenomena, the forces ζ_m are dependent on the deformation. For this reason, it is more suitable to move from the Lagrangian to the Eulerian coordinates. So that Equation (50) can be rewritten as:

$$\mathbf{j}_m = \sum_{k=s,1,\dots,N}\frac{L_{mk}J^{-1}}{T}\mathbb{B}\nabla\mu_k = \sum_{k=s,1,\dots,N}\ell_{mk}\nabla\mu_k. \tag{101}$$

where the coefficient ℓ_{mk} are now constant, i.e. they are independent of the deformation. These can be correlated to drag coefficients, which are commonly used in the theory of mixtures [41,42]. Let us first rewrite the fluxes as $\mathbf{j}_m = c_m(\mathbf{v}_m - \mathbf{v}_n) = c_m\bar{\mathbf{v}}_m$, where $\mathbf{v}_m$ is the velocity of the m-th component in the current configuration, $\mathbf{v}_n$ is the velocity of the network also in the current configuration and $\bar{\mathbf{v}}_m$ is the relative velocity of the m-th component with respect to the network. If now invert Equations (101), we obtain the following linear system:

$$-c_j\nabla\mu_j = \sum_m h_{jm}\bar{\mathbf{v}}_m = \sum_{i\neq j} f_{ji}\left(\bar{\mathbf{v}}_j - \bar{\mathbf{v}}_i\right) + f_{js}(\bar{\mathbf{v}}_j - \bar{\mathbf{v}}_s) + f_{jn}\bar{\mathbf{v}}_j, \tag{102}$$

$$-c_s\nabla\mu_s = \sum_i f_{si}\left(\bar{\mathbf{v}}_s - \bar{\mathbf{v}}_i\right) + f_{sn}\bar{\mathbf{v}}_s, \tag{103}$$

where $j = 1\dots N$, f_{mb} are the drag coefficients related to the interaction between the phase $m = s, 1, \cdots, N$ and the phase $b = n, s, 1, \cdots, N$. Based on the Onsanger's reciprocal relation we have that:

$$f_{mb} = f_{bm} \qquad m, b \in \{s, 1, \cdots, N\}. \tag{104}$$

A common assumption in the study of mixture theory is that the solute-solute drag can be neglected so that $f_{ij} = 0$ for $i, j = 1, \ldots, N$ [26,41]. The remaining drag coefficient are instead defined by:

$$f_{sn} = \frac{1}{k}, \quad f_{js} = \frac{k_B T c_j}{D_j^0}, \quad f_{js} + f_{jn} = \frac{k_B T c_j}{D_j}, \tag{105}$$

where k is the hydraulic permeability of the solvent in the network, D_j^0 is the diffusion coefficient of the solute in pure solution, while D_j is the diffusion coefficient in the gel.

Using (102)-(105), the relative velocities are of the form:

$$\bar{\mathbf{v}}_s = -K \left(\nabla \mu_s + \sum_i \frac{D_i}{D_i^0} \frac{C_i}{C_s} \nabla \mu_i \right), \tag{106}$$

$$\bar{\mathbf{v}}_j = -\frac{D_j}{k_B T} \nabla \mu_j + \frac{D_j}{D_j^0} \bar{\mathbf{v}}_s, \tag{107}$$

and the coefficient K is defined as:

$$\frac{1}{K} = \frac{1}{c_s k} + \sum_i \frac{k_B T}{D_i^0} \left(1 - \frac{D_i}{D_i^0} \right) \frac{C_i}{C_s}. \tag{108}$$

If we now move back to the initial configuration, we have that the fluxes $\mathbf{J}_m$ have the form:

$$\mathbf{J}_m = J \mathbb{F}^{-1} \mathbf{j}_m = J \mathbb{F}^{-1} c_m \bar{\mathbf{v}}_s, \tag{109}$$

where $\bar{\mathbf{v}}_s$ are defined by Equations (106)-(107). Substituting now Equations (109) into the conservation of mass laws (13), we recover the governing equations (51)-(52) in Section (4.5).

D Model B: Separating the Volumetric Deformation.

The derivation of the governing equation for the second model proposed follow the same steps as model A, with only few changes. The conservation laws (Section 4.1) are still valid as they do not depend on the specific kinetics model chosen. As discussed in Section 4.2, we use multiplicative decomposition to isolate the different contribution to the strain:

$$\mathbb{F} = \bar{\mathbb{F}} \mathbb{F}_{vol} = J^{1/3} \bar{\mathbb{F}}_e \bar{\mathbb{F}}_v, \tag{110}$$

where we have used the fact that $\mathbb{F}_{vol} = J^{1/3} \mathbb{I}$, with $J = \det \mathbb{F}$. Where both $\bar{\mathbb{F}}_e$ and $\bar{\mathbb{F}}_v$ preserve the ECM volume. Consequently, analogously to Equation (24), we have that:

$$\det \bar{\mathbb{F}}_v = 1. \tag{111}$$

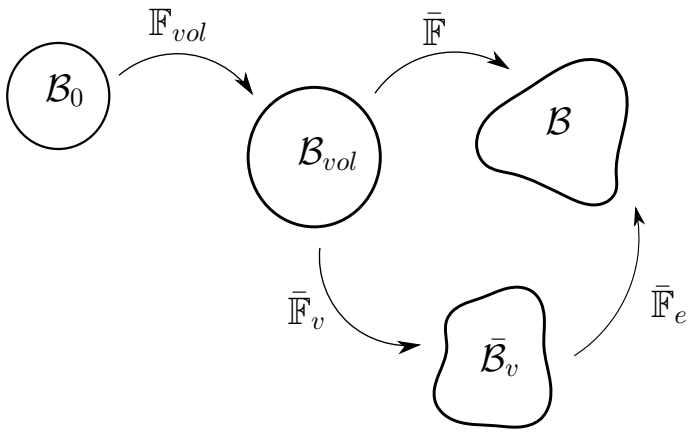

Fig. 12: Multiplicative decomposition of Model B

Besides the viscous velocity gradient $\bar{\mathbb{L}}_v = \dot{\bar{\mathbb{F}}}_v \bar{\mathbb{F}}_v^{-1}$, we also define the total velocity gradient $\mathbb{L} = \dot{\mathbb{F}}\mathbb{F}^{-1}$. These are the two variables we will be using to describe the kinetics of the solid phase deformation.

Focusing on the reversible exchange of energy and mass between the system and the environment, we have that Equation (25) and (26) still hold, so that the energy imbalance inequality can still be written as Equation (29). Note however that the constitutive function of the free energy is now of the form:

$$\psi = \psi(\bar{\mathbb{F}}, \bar{\mathbb{F}}_e, J, C_s, C_i, \mathbf{H}), \tag{112}$$

where J needs now to be introduced to the list of independent variables.

If we now take the time derivative of J, $\bar{\mathbb{F}}$ and $\bar{\mathbb{F}}_e$, we have that:

$$\dot{J} = J(\mathbb{I} : \mathbb{L}), \tag{113}$$

$$\dot{\bar{\mathbb{F}}} = J^{-1/3}\mathbb{L}\mathbb{F} - \frac{1}{3}J^{-1/3}(\mathbb{I} : \mathbb{L})\mathbb{F}, \tag{114}$$

$$\dot{\bar{\mathbb{F}}}_e = \mathrm{DEV}[\mathbb{L}]\bar{\mathbb{F}}_e - \bar{\mathbb{F}}_e\bar{\mathbb{L}}_v, \tag{115}$$

so that the dynamics of the system can be fully described in terms of $\mathbb{L}$ and $\bar{\mathbb{L}}_v$. If we combine Equations (112)-(115) with the energy inequality (29), we obtain:

$$\begin{aligned}\left(\frac{\partial\psi}{\partial C_s} - \mu_s + p v_s\right)\dot{C}_s + \sum_i \left(\frac{\partial\psi}{\partial C_i} + e\Phi z_i - \mu_i\right)\dot{C}_i + \left(\frac{\partial\psi}{\partial \mathbf{H}} - \mathbf{E}\right)\cdot\dot{\mathbf{H}} \\ + \left(\mathrm{DEV}\left[J^{-1/3}\frac{\partial\psi}{\partial\bar{\mathbb{F}}}\mathbb{F}^T + \frac{\partial\psi}{\partial\bar{\mathbb{F}}_e}\bar{\mathbb{F}}_e^T\right] - \mathbb{S}\mathbb{F}^T + J\left(\frac{\partial\psi}{\partial J} - p\right)\mathbb{I}\right) : \mathbb{L} \\ + \sum_m \nabla_0\,\mu_m \cdot \mathbf{J}_m - \mathrm{DEV}[\bar{\mathbb{M}}_e] : \bar{\mathbb{L}}_v \leq 0.\end{aligned} \tag{116}$$

Moving on to the form of the free energy ψ (see Section 4.4), Equations (34)-(37) still holds. On the other hand, the last term, i.e. the strain energy ψ_5, needs

to be update so to have a term explicitly related to the volumetric deformation, which we assume to be perfectly elastic. From a rheological point of view, as illustrated in Figure 13a, this is equivalent to add a spring in series to the "circuit" in Figure 6a.

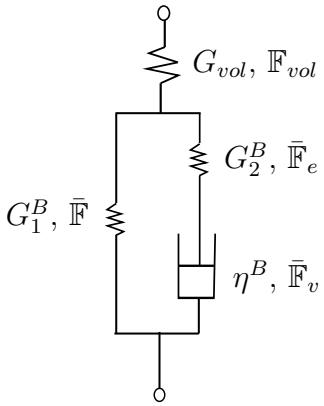

(a)

Element	**Constitutive Properties**	**Deformation**
spring *vol*	Isotropic Neo-Hookean spring	volumetric
spring 1	Isotropic Neo-Hookean spring	deviatoric
spring 2	Isotropic Neo-Hookean spring	deviatoric
dashpot	Isotropic Linear dashpot	deviatoric

(b)

Fig. 13: (a) Schematic representation of the non-linear rheological model for ECM; (b) Table summarizing the major properties of the model components.

As in Section 4.4, we can decompose strain energy as the sum of contributions from each element in the rheological model:

$$\psi_5 = \psi_{5.1}(\bar{\mathbb{F}}) + \psi_{5.2}(\bar{\mathbb{F}}_e) + \psi_{vol}(J). \tag{117}$$

which based on the constitutive properties list in Table (13b) have the form:

$$\psi_{5.1}(\bar{\mathbb{F}}) = \frac{G_1^B}{2}\left(\bar{\mathbb{F}} : \bar{\mathbb{F}} - 3\right), \tag{118}$$

$$\psi_{5.2}(\bar{\mathbb{F}}_e) = \frac{G_2^B}{2}\left(\bar{\mathbb{F}}_e : \bar{\mathbb{F}}_e - 3\right), \tag{119}$$

$$\psi_{vol}(J) = \frac{G_{vol}}{2}\left[3(J^{2/3} - 1) - \ln J^2\right]. \tag{120}$$

Following the same argument as in Appendix (B), we have that the term highlighted in blue in Equation (116) must be identically zero. This leads to

following set of governing equations:

$$\mu_s = pv_s + \mu_s^0 + kT\left[\ln\frac{C_s v_s}{1+C_s v_s} + \frac{1}{1+C_s v_s} + \frac{\chi}{(1+C_s v_s)^2} - \sum_i \frac{C_i}{C_s}\right], \tag{121}$$

$$\mu_i = \mu_i^0 + e\Phi z_i + kT\ln\frac{C_i}{C_s}, \tag{122}$$

$$\mathbf{E} = \frac{1}{\epsilon J}\mathbb{F}^T\mathbb{F}\,\mathbf{H}\,, \tag{123}$$

$$\mathbb{T} = \left(G_{vol}\frac{J^{2/3}-1}{J} - p\right)\mathbb{I} + \frac{G_1^B}{1+C_s v_s}\mathrm{DEV}[\bar{\mathbb{B}}] + \frac{G_2^B}{1+C_s v_s}\mathrm{DEV}[\bar{\mathbb{B}}_e] + \epsilon\left[\frac{1}{2}|\nabla\Phi|^2\mathbb{I} - \nabla\Phi\otimes\nabla\Phi\right], \tag{124}$$

When looking at how energy is dissipated, the derivation in Section (4.5) and Appendix C is still valid once replacing $\mathbb{L}_v \leftrightarrow \bar{\mathbb{L}}_v$ and $\mathbb{C}_e \leftrightarrow \bar{\mathbb{C}}_e$. Thus Equation (98) is now of the form:

$$\bar{\mathbb{L}}_v = \frac{G_2^B}{\eta^B}\mathrm{DEV}[\bar{\mathbb{C}}_e]. \tag{125}$$

If we assume that the time of relaxation τ_R is independent of the model used (see Equation (99)), this yield to a system of governing equations analogous to the System (51)- (53):

$$\partial_t C_s = \nabla_0\cdot\left[K\mathbb{F}^{-1}\left(C_s\nabla\mu_s + \sum_i \frac{D_i}{D_i^0}C_i\nabla\mu_i\right)\right], \tag{126}$$

$$\partial_t C_i = \nabla_0\cdot\left[\frac{D_i}{k_B T}C_i\mathbb{F}^{-1}\nabla\mu_i - \frac{D_i}{D_i^0}\frac{C_i}{C_s}\mathbf{J}_s\right], \tag{127}$$

$$\dot{\bar{\mathbb{B}}}_e = \bar{\mathbb{B}}_e\bar{\mathbb{L}}^T + \bar{\mathbb{L}}\bar{\mathbb{B}}_e - \frac{1}{\tau_R}\bar{\mathbb{B}}_e\mathrm{DEV}\left[\bar{\mathbb{B}}_e\right]. \tag{128}$$

To sum up, model A and model B are similar with only exception of the state equation for the Cauchy stress $\mathbb{T}$ and the governing equation of the dashpot.

E Simulation Parameters.

In this Section we list the values of the known parameters used in the Sections (6.1) and (7.1). This are from [42], and refer to the experiment by Netti et al. [34,42].

Symbol	Value	Unit
C_f	3.947×10^{23}	m^{-3}
v_s	3×10^{-29}	m^3
z_f	-4	-
k_B	1.38×10^{-23}	J/K
T	295	K
c_0	9.27×10^{25}	m^{-3}

Table 3: Parameters adopted in the simulations as estimated in [42] in reference to the experiment by Netti et al. [34].

F Free Swelling

We here derive the equilibrium equation for free swelling. In this case, we have that the tensors $\mathbb{F}_e$ and $\bar{\mathbb{F}}_e$ have diagonal form:

$$\mathbb{F}_e = \lambda_e \mathbb{I}, \quad \bar{\mathbb{F}}_e = \bar{\lambda}_e \mathbb{I}. \tag{129}$$

Based on Equation (98) in Appendix C, we have that the viscous contribution vanish so that $\mathbb{B}_e = \mathbb{B} = \lambda^2 \mathbb{I}$, while $\bar{\mathbb{B}}_e = \mathbb{I}$. Substituting these results and the equilibrium condition (66)-(67) into the model equations (see Table 1 in Section 4.5 for the full list) and setting all spatial derivatives to zero, we have that:

$$p = \begin{cases} \dfrac{G_1^A + G_2^A}{1 + C_s v_s}(\lambda^2 - 1) & \text{MODEL A,} \\ \dfrac{G_{vol}}{1 + C_s v_s}(\lambda^2 - 1) & \text{MODEL B,} \end{cases} \tag{130}$$

$$\Pi_{osm} = \frac{k_B T}{v_s}\left[\ln \frac{C_s v_s}{1 + C_s v_s} + \frac{1}{1 + C_s v_s} + \frac{\chi}{(1 + C_s v_s)^2}\right], \tag{131}$$

$$\Pi_{ion} = k_B T \left(\frac{C_+}{v_s C_s} + \frac{C_-}{v_s C_s} - 2c^0\right), \tag{132}$$

$$0 = \frac{v_s}{k_B T}(p + \Pi_{osm} - \Pi_{ion}), \tag{133}$$

$$0 = \pm \frac{e}{k_B T}\phi + \ln \frac{C_\pm}{C_s v_s c_\pm^0}, \qquad i = 1, \ldots, N, \tag{134}$$

$$Q = e\,(C_+ - C_- + z_f C_f) = 0, \tag{135}$$

where Π^n and Π_A^{ion} are the osmotic pressures due to the mixing of the polymer network with the solvent and the imbalance of ions inside and outside the ECM. Note that at equilibrium the system reaches a balance between the mechanical pressure p_A and the osmotic pressures. Moreover, the electro-neutrality condition is naturally imposed, Equation (135).

Using Equations (134), we recover the well known Donnan Equilibrium [16]:

$$C_+C_- = (v_s C_s c_0)^2. \tag{136}$$

Considering now Equations (135)-(136), we have that at equilibrium C_+, C_- and ϕ satisfy:

$$C_\pm = \frac{1}{2}\left[\mp z_f C_f + \sqrt{(z_f C_f)^2 + (2v_s C_s c_0)^2}\right], \tag{137}$$

$$\phi = \frac{kT}{2e}\ln\frac{C_-}{C_+}. \tag{138}$$

Finally, if we substitute Equations (131)-(132) and (136)-(138) into (133), we are left with a single equilibrium condition that implicitly defines λ:

$$\begin{aligned} F(\lambda) =& \frac{\lambda^3+\chi}{\lambda^6} + \frac{pv_s}{k_BT} + \ln\frac{\lambda^3-1}{\lambda^3} + 2c_0v_s \\ &- \sqrt{\left(\frac{z_fC_fv_s}{\lambda^3-1}\right)^2 + 4v_s^2c_0^2} = 0. \end{aligned} \tag{139}$$

References

1. Anand, L.: A thermo-mechanically-coupled theory accounting for hydrogen diffusion and large elastic–viscoplastic deformations of metals. International Journal of Solids and Structures **48**(6), 962 – 971 (2011)
2. Benaglia, S., Gisbert, V.G., Perrino, A., Amo, C.A., Garcia, R.: Fast and high-resolution mapping of elastic properties of biomolecules and polymers with bimodal afm. Nature Protocols **13**, 2890–2907 (11 2018)
3. Benfenati, F., Beretta, G.P.: Ergodicity, Maximum Entropy Production, and Steepest Entropy Ascent in the Proofs of Onsager's Reciprocal Relations. Journal of Non Equilibrium Thermodynamics **43**, 101–110 (Apr 2018)
4. Beretta, G.P.: The fourth law of thermodynamics: steepest entropy ascent. arXiv preprint arXiv:1908.05768 (2019)
5. Bergström, J., Boyce, M.: Constitutive modeling of the large strain time-dependent behavior of elastomers. Journal of the Mechanics and Physics of Solids **46**(5), 931 – 954 (1998)
6. Boyce, M.C., Arruda, E.M.: Constitutive models of rubber elasticity: A review. Rubber Chemistry and Technology **73**(3), 504–523 (2000)
7. Buenger, D., Topuz, F., Groll, J.: Hydrogels in sensing applications. Progress in Polymer Science **37**(12), 1678 – 1719 (2012)
8. Butcher, D., Alliston, T., Weaver, V.: A tense situation: forcing tumour progression. nat rev cancer 9: 108-122. Nature reviews. Cancer **9**, 108–22 (03 2009)
9. Caccavo, D., Cascone, S., Lamberti, G., Barba, A.A.: Hydrogels: experimental characterization and mathematical modelling of their mechanical and diffusive behaviour. Chem. Soc. Rev. **47**, 2357–2373 (2018)
10. Caccavo, D., Vietri, A., Lamberti, G., Barba, A.A., Larsson, A.: Modeling the mechanics and the transport phenomena in hydrogels. In: Manca, D. (ed.) Quantitative Systems Pharmacology, Computer Aided Chemical Engineering, vol. 42, chap. 12, pp. 357 – 383. Elsevier (2018)
11. Chaudhuri, O.: Viscoelastic hydrogels for 3d cell culture. Biomater. Sci. **5**, 1480–1490 (2017)
12. Cohen Stuart, M., Huck, W., Genzer, J., Müller, M., Ober, C., Stamm, M., Sukhorukov, G., Szleifer, I., Tsukruk, V., Urban, M., Winnik, F., Zauscher, S., Luzinov, I., Minko, S.: Emerging applications of stimuli-responsive polymer materials. Nature materials **9**, 101–13 (2010)
13. Deligkaris, K., Tadele, T.S., Olthuis, W., Van den Berg, A.: Hydrogel-based devices for biomedical applications. Sensors and Actuators B: Chemical **147**, 765–774 (2010)
14. Doi, M.: Soft Matter Physics. OUP Oxford (2013)
15. Drozdov, A.: Swelling of ph-responsive cationic gels: Constitutive modeling and structure–property relations. International Journal of Solids and Structures **64-65**, 176 – 190 (2015)
16. Drozdov, A.D., deClaville Christiansen, J., Sanporean, C.G.: Inhomogeneous swelling of ph-responsive gels. International Journal of Solids and Structures **87**, 11 – 25 (2016)
17. Flory, P.J.: Thermodynamics of high polymer solutions. The Journal of Chemical Physics **10**(1), 51–61 (1942)
18. Flory, P.: Principles of Polymer Chemistry. Baker lectures 1948, Cornell University Press (1953)

19. Garcia-Gonzalez, D., Jerusalem, A.: Energy based mechano-electrophysiological model of cns damage at the tissue scale. Journal of the Mechanics and Physics of Solids **125**, 22 – 37 (2019)
20. Garcia-Gonzalez, D.: Magneto-visco-hyperelasticity for hard-magnetic soft materials: theory and numerical applications. Smart Materials and Structures **28**(8), 085020 (jul 2019)
21. Gurtin, M.E.: Generalized ginzburg-landau and cahn-hilliard equations based on a microforce balance. Physica D: Nonlinear Phenomena **92**(3), 178 – 192 (1996)
22. Hennessy, M.G., Münch, A., Wagner, B.: Surface induced phase separation of a swelling hydrogel (2018), preprint on webpage `http://www.wias-berlin.de/preprint/2562/wias_preprints_2562.pdf`
23. Hong, W.: Continuum Models of Stimuli-responsive Gels, pp. 165–196. Springer Berlin Heidelberg, Berlin, Heidelberg (2012)
24. Hu, Y., Suo, Z.: Viscoelasticity and poroelasticity in elastomeric gels. Acta Mechanica Solida Sinica **25**(5), 441 – 458 (2012)
25. Huggins, M.L.: Some properties of solutions of long-chain compounds. The Journal of Physical Chemistry **46**(1), 151–158 (1942)
26. Katzir-Katchalsky, A., Curran, P.: Nonequilibrium thermodynamics in biophysics. Books in Biophysics, Harvard University Press (1965)
27. Kondepudi, D., Prigogine, I.: Modern Thermodynamics: From Heat Engines to Dissipative Structures. CourseSmart, John Wiley & Sons (2014)
28. Kröner, E.: Allgemeine Kontinuumstheorie der Versetzungen und Eigenspannungen. Archive for Rational Mechanics and Analysis **4**, 273–334 (1959)
29. Lebon, G., Jou, D., José, C.V.: Understanding Non-Equilibrium Thermodynamics. Springer-Verlag Berlin Heidelberg (01 2008)
30. Levental, I., Georges, P.C., Janmey, P.A.: Soft biological materials and their impact on cell function. Soft Matter **3**, 299–306 (2007)
31. Li, J., Mooney, D.: Designing hydrogels for controlled drug delivery. Nature Reviews Materials **1**, 16071 (2016)
32. Lubarda, V.A.: Constitutive theories based on the multiplicative decomposition of deformation gradient: Thermoelasticity, elastoplasticity, and biomechanics. Applied Mechanics Reviews **57**(2), 95–108 (04 2004)
33. Marsland, R., England, J.: Limits of predictions in thermodynamic systems: a review. Reports on Progress in Physics **81**(1) (2017)
34. Netti, P.A., Berk, D.A., Swartz, M.A., Grodzinsky, A.J., Jain, R.K.: Role of extracellular matrix assembly in interstitial transport in solid tumors. Cancer Research **60**(9), 2497–2503 (2000)
35. N'Guyen, T., Lejeunes, S., Eyheramendy, D., Boukamel, A.: A thermodynamical framework for the thermo-chemo-mechanical couplings in soft materials at finite strain. Mechanics of Materials **95**, 158 – 171 (2016)
36. Onsager, L.: Reciprocal relations in irreversible processes. i. Phys. Rev. **37**, 405–426 (Feb 1931)
37. Paszek, M.J., Zahir, N., Johnson, K.R., Lakins, J.N., Rozenberg, G.I., Gefen, A., Reinhart-King, C.A., Margulies, S.S., Dembo, M., Boettiger, D., Hammer, D.A., Weaver, V.M.: Tensional homeostasis and the malignant phenotype. Cancer Cell **8**(3), 241 – 254 (2005)
38. Prigogine, I.: Introduction to thermodynamics of irreversible processes. Interscience Publishers (1968)
39. Sun, D.N., Gu, W.Y., Guo, X.E., Lai, W.M., Mow, V.C.: A mixed finite element formulation of triphasic mechano-electrochemical theory for charged, hydrated bi-

ological soft tissues. International Journal for Numerical Methods in Engineering **45**(10), 1375–1402 (1999)
40. Xue, S.L., Li, B., Feng, X.Q., Gao, H.: Biochemomechanical poroelastic theory of avascular tumor growth. Journal of the Mechanics and Physics of Solids **94**, 409 – 432 (2016)
41. Xue, S.L., Li, B., Feng, X.Q., Gao, H.: A non-equilibrium thermodynamic model for tumor extracellular matrix with enzymatic degradation. Journal of the Mechanics and Physics of Solids **104**, 32 – 56 (2017)
42. Xue, S.L., Lin, S.Z., Li, B., Feng, X.Q.: A nonlinear poroelastic theory of solid tumors with glycosaminoglycan swelling. Journal of Theoretical Biology **433**, 49 – 56 (2017)
43. Yu, Y., Landis, C.M., Huang, R.: Salt-Induced Swelling and Volume Phase Transition of Polyelectrolyte Gels. Journal of Applied Mechanics **84**(5) (03 2017)